Sādhanā, Vol. 12, Parts 1 & 2, February 1988, pp. 45–104. © Printed in India.

Shock-wave-turbulent-boundary-layer interaction and its control: A survey of recent developments

P R VISWANATH

Aerodynamics Division, National Aeronautical Laboratory, Wind Tunnel Centre, Bangalore 560 017, India

Abstract. This paper presents an overview of some of the recent developments that have taken place in the understanding, prediction and control of two-dimensional shock-wave-turbulent-boundary-layer interaction at high speeds. Following a brief description of the upstream influence phenomena, detailed discussions of incipient and fully separated flows at supersonic and transonic speeds are presented. A brief account of certain gross unsteady features of shock-separated flows is given next. Typical examples demonstrating the current ability to predict these complex flows are also included. Finally, a review of techniques using suction and tangential blowing for controlling shock-separated flows is presented.

Keywords. Shock-wave-boundary-layer interaction; boundary layer control; viscous-inviscid interaction.

1. Introduction

The subject of shock-wave-boundary-layer interaction continues to be an important area of research in view of its many applications in both external and internal aerodynamics. Shock-wave-boundary-layer interactions occur on airfoils and in turbo-machinery blades in transonic flow, in supersonic intakes, and ahead of control surfaces and flares in supersonic flow, to cite just a few of the applications. Flow separation, often associated with these interactions, generally leads to increased energy losses in the system and degrades the performance of the aerodynamic device; flow unsteadiness, often a result of separation, can cause additional problems (e.g. wing buffeting, air intake buzz etc.) which are undesirable in practice. Separation control by some active or passive means, in general, is beneficial for improving the performance of the device under consideration.

It is now over three decades since the early investigations on shock-boundary layer interaction were reported. These include the studies of Liepmann (1946), Ackeret *et al* (1946), and Liepmann *et al* (1951) from which emerged many important observations on the nature of these interactions with laminar and turbulent boundary layers at transonic speeds. Pearcey (1961, pp. 1164–1344) provided an excellent summary of earlier work on the subject of transonic interactions on

A list of symbols is given at the end of the paper.

airfoils and their control. Following these, research shifted to the supersonic/hypersonic regimes as a result of increasing speeds of aircraft and developments in space flight. In the last two decades, considerable experimental and theoretical research has been carried out on the many aspects of this complex fluid dynamical problem. This has led to some degree of understanding on the nature of these interactions, and in identifying some of the important parameters affecting the phenomena in the different speed regimes. While there has been significant progress made in the understanding and analysis of laminar interactions, in general, the structure of turbulent interactions is still poorly understood; progress is hampered by our inadequate understanding of the dynamics of turbulence, particularly in the presence of adverse pressure gradients. In spite of these limitations, several engineering calculation methods, of varying degrees of complexity and sophistication, have emerged for predicting these flows even when there are small regions of separation.

This paper presents an overview of some of the important developments that have taken place in the understanding, prediction and control of these complex interactions. This article is not intended to be a critical review of all aspects or an exhaustive survey of relevant papers in the published literature. Following Green's (1970, pp. 235–340) review paper, quite a few survey papers covering various aspects of the problem have appeared (Charwat 1970, pp. 1–132; Stanewsky 1973; Sirieix 1975; Brusseleers 1980; Adamson & Messiter 1980), the most recent being that of Delery (1985); these publications may be referred to for more details. The emphasis in this paper is on turbulent interactions because of their importance in practical applications. Since most of the investigations have been carried out on two-dimensional flows, the discussions to follow are limited primarily to two-dimensional interactions, and without heat transfer at the wall (the adiabatic case). In reality, shock-wave-boundary-layer interactions occur under rather complex circumstances, for example, involving surface curvature, heat transfer at the wall, nonuniform approaching flow and three-dimensionality. With the idea of understanding some of the basic features of these interactions, most investigations have been carried out on relatively simple model geometries with the boundary layer developing on a flat plate ahead of the interaction. These interactions have often been referred to as 'basic interactions' and will form the major part of the material in this paper.

The paper begins with a brief discussion of the upstream influence phenomena which is followed by detailed discussion of incipient and fully separated flows at supersonic speeds. Features of certain transonic shock-wave-boundary-layer interactions are discussed next. A brief account of certain gross unsteady features of shock-induced separated flows is given, although the data available is still very meagre. Typical examples, demonstrating the current state of calculation methods, are included. Finally, a discussion of techniques employing suction and injection (or blowing) for controlling these separated flows are presented.

2. The mechanism of upstream influence in shock-boundary layer interaction

In inviscid supersonic flow, it is well-known that when a shock wave meets (or is generated at) the surface, the surface pressure changes discontinuously through the

shock (figure 1). However, with a boundary layer developing on the wall, such a discontinuous pressure rise cannot occur because of the presence of the subsonic part of the boundary layer close to the wall, which cannot support an abrupt pressure rise. As a result, the pressure disturbances imposed by the shock are propagated partly upstream and partly downstream on the surface. The thickening of the subsonic stream tubes, in reaction to the adverse pressure gradients imposed by the shock, generate compression waves in the supersonic part of the boundary layer. These waves cause additional pressure rise and lead to further readjustment in the subsonic part of the boundary layer. This process continues and an equilibrium is reached so that the gradual pressure rise in the subsonic part of the boundary layer is compatible with the rather discontinuous pressure rise in the outer inviscid flow.

If the overall pressure rise across is not large, the boundary layer may not separate. Under these conditions, the interaction is termed 'weak' implying that the outer inviscid flow and the resulting shock pattern are only weakly altered (figure 1). On the other hand, if the total pressure rise associated with the shock system is large, boundary layer separation occurs causing significant perturbations in the outer flow as well as in the wave system (figure 1). These interactions are termed 'strong' implying strong coupling between the inviscid and the viscous part of the flow-field.

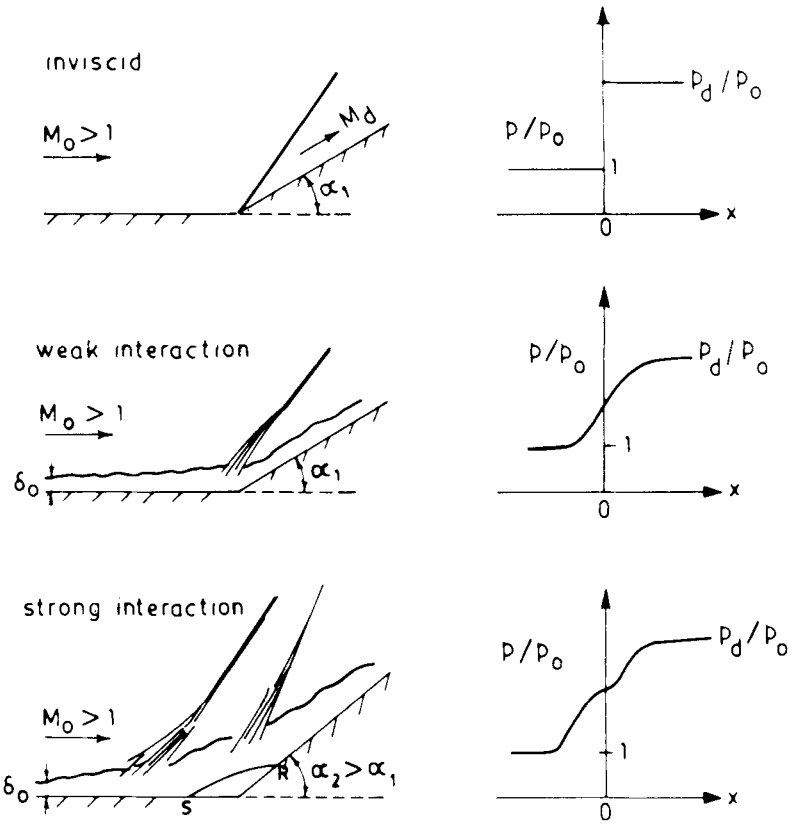

Figure 1. Schematic of wave pattern and wall pressure distributions at a compression corner.

The shock-wave-boundary-layer interaction zone, which in general depends on the nature of the boundary layer, the flow conditions upstream of the shock and the overall shock pressure rise, can extend over several boundary-layer thicknesses. With a laminar boundary layer, the interaction zone can be several times longer than the corresponding turbulent case for the same overall pressure rise.

3. Supersonic interactions without extended separation

3.1 *Interaction without separation*

If the total pressure rise associated with the shock system is either small or moderate, the boundary layer can negotiate the pressure gradients without separating. Typical examples of weak interactions for the cases of a compression corner and an impinging shock wave are shown in figure 2. The pressure rise occurs typically over a distance of 2–3 boundary layer thicknesses for the turbulent case. In the inner subsonic region of the boundary layer, shear stress gradients normal to the wall are important, while in the outer supersonic part the flow is largely inviscid. A (weak) secondary wave system is generally formed as a result of the interaction (shown dotted in figure 2). In the case of the compression corner, the secondary wave system results partly from the streamline curvature arising from thickening of the subsonic stream tubes and partly by the refraction of the outgoing compressive waves which generate waves that get reflected at the sonic line. For the case of the impinging shock wave, a second (secondary) wave system is formed due to the refraction of the incident shock. The wave pattern in the outer supersonic part of the boundary layer is essentially due to its vorticity or rotationality. This process is described in detail by Henderson (1967). The boundary layer thickness decreases across the interaction since a large fraction of the boundary layer flow is supersonic.

3.2 *Nature of turbulent separation*

Before addressing the problem of incipient separation, it is important and instructive to include a brief discussion of a fundamental feature of the turbulent separation process. Unlike in the case of steady laminar flows, turbulent boundary layer separation involves a gradual process before becoming separated in a time-averaged sense. Fully developed (or time-averaged) separation occurs where the mean wall shear stress is zero and flow downstream involves regions of back or reversed flow ($u < 0$).

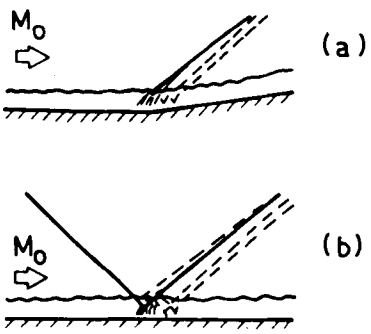

Figure 2. Schematic of wave pattern without separation (from Green 1970), (**a**) compression corner, (**b**) incident shock.

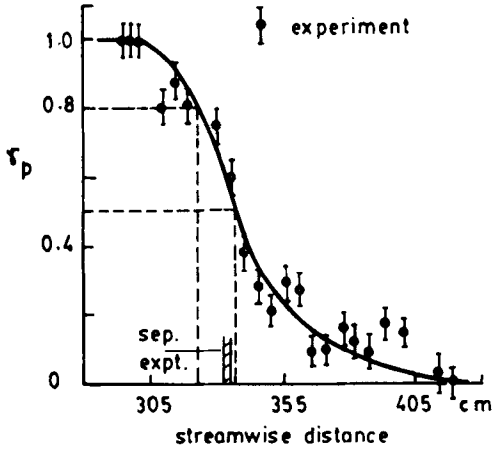

Figure 3. Velocity intermittency near the wall (from Simpson *et al* 1977).

It is now well-established (Sandborn & Kline 1961; Simpson *et al* 1977) that turbulent boundary layer separation exhibits intermittent reversed flow near the wall much ahead of the time-averaged separation point; this upstream zone has been termed the intermittent separation region. Measurements (Simpson *et al* 1977) related to this unsteady behaviour of separation in the case of a low speed separated flow on a flat plate is illustrated in figure 3, along with the associated boundary layer edge velocity distribution in figure 4. Laser velocimeter measurements of intermittency, γ_p (defined as the fraction of the time the flow is in the downstream direction, $U > 0$), at a location near the wall, is plotted against streamwise distance. After a careful examination of low speed data, values of γ_p near the wall of about 0·8 and 0·5, for the onset of intermittent separation and fully developed separation, respectively, have been suggested (e.g. Simpson *et al* 1977); the pressure gradient relief appears to follow the beginning of intermittent separation. Measurements of γ_p in transonic separated flows have also revealed features qualitatively similar to low speed flows (Delery 1981; Viswanath & Brown 1983); a further discussion of this aspect is contained in § 5.

3.3 *Incipient separation*

As the overall pressure rise across the shock system is increased, a situation is reached which marks the beginning of a tiny separated region or a bubble. In the

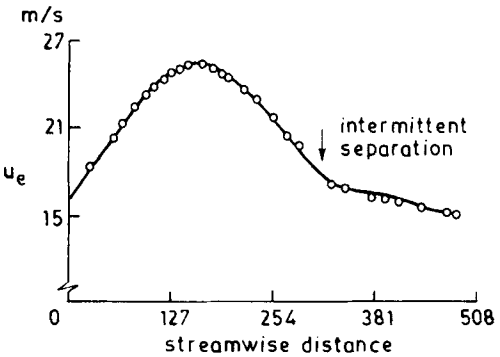

Figure 4. Boundary layer edge velocity distribution (from Simpson *et al* 1977).

literature, considerable emphasis has been given to a rather (hypothetical) condition in which the mean wall shear stress is positive everywhere except at one location (or a narrow region), where it is vanishingly small. This flow condition has been referred to as incipient separation (IS). From a practical or design view point, it is important to know what conditions lead to incipient separation, since it marks, in some sense, the onset of adverse effects.

Experimental determination of IS has not been easy because of the difficulties in accurately measuring rather small values of wall shear stress in a region of strong adverse pressure gradient. As a result, investigators in the past have proposed and employed several indirect techniques to identify IS. The emphasis has been to identify the onset of a small bubble or some marked change in the flow pattern. As we shall see in the next section, the use of different techniques have partly contributed to a somewhat confusing picture in the understanding of the IS phenomena, and the Reynolds number effects, in particular.

Kuehn (1959) proposed the appearance of a kink or a triple inflection point in the surface pressure distributions as a condition for IS. Another common method involves extrapolation of a measure of the bubble size to zero value from a series of experimental surface pressure distributions, which range from fully attached to fully separated conditions. The bubble size (in the streamwise direction) can be obtained, for example, from a surface oil flow technique. The first appearance of a 'separation' or an 'induced shock wave' as seen in a Schlieren/shadowgraph has often been adopted to identify IS. The orifice dam technique, which is intrusive, has been employed to detect surface flow direction. The various methods that have been used, their merits and shortcomings are discussed by Settles *et al* (1976a).

3.4 *Pressure rise to incipient separation*

Determination of the pressure rise associated with IS has been the subject of several investigations. The relevant parameters of the problem include the Mach number ahead of the interaction, M_o, a characteristic Reynolds number of the boundary layer flow and the geometry of the shock generator. For boundary layers developing in a zero pressure gradient upstream of the interaction, shape factor effects are related through the Reynolds number; also, the boundary layer thickness δ_o has been found to be a useful length scale. Although incipient separation data exist from many different sources involving different shock generators, reliable data covering a wide range of Reynolds number are only available for a compression corner (or ramp) geometry around $M_o = 3{\cdot}0$. Figure 5 shows these results (Settles *et al* 1976a) in a plot of α_{is}, the ramp angle at which a tiny bubble is formed, as a function of Re_{δ_o}; the pressure rise at IS can be calculated from M_o and α_{is}.

In the lower Reynolds number range ($10^4 < Re_{\delta_o} < 10^5$), α_{is} shows a decreasing trend, which is consistent with the free interaction principle (to be discussed in § 4). For $Re_{\delta_o} > 10^5$, mixed trends are seen; the data of Roshko & Thomke (1969, pp. 109–138) and Law (1974) show an increasing trend, while the data of Settles *et al* (1976) show little or no variation with increased Re_{δ_o}. The data of Settles and coworkers cover a wide range of Re_{δ_o} and the near constancy of α_{is} is observed for all the different techniques employed by them. For the data shown in figure 5 no systematic variation of H with Re_{δ_o} is observed (figure 6) suggesting weaker effects, if any, of H on α_{is} in the range of Re_{δ_o} considered.

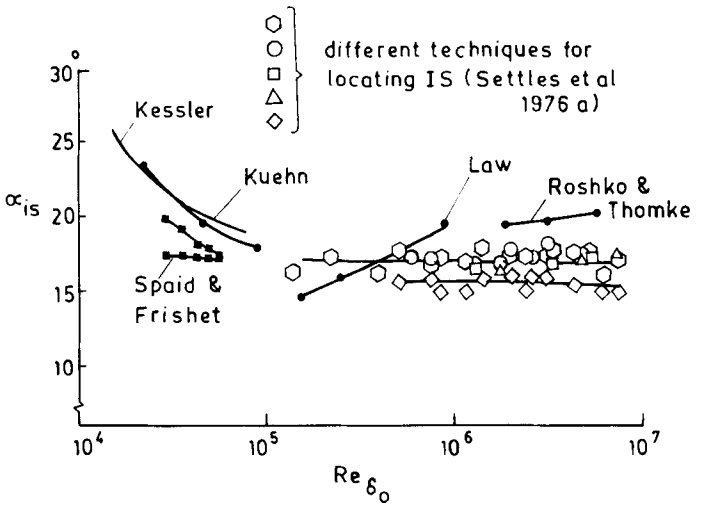

Figure 5. Reynolds number effect on incipient separation at a compression corner: M_o = 2·9 (from Settles *et al* 1976a).

Satisfactory explanation for the observed reversal in the trend of α_{is} vs. Re_{δ_o}, seen at the higher Reynolds number (for some of the data in figure 5), still does not exist; although certain speculations have been made (Elfstrom 1972; Roshko & Thomke 1969, pp. 109–138). Settles *et al* (1976a) have provided some explanation in favour of their observations. They suggest that the IS phenomenon is a gradual transition between attached and fully separated flow and does not involve an abrupt change; therefore a small spread in α_{is} values (about 3°, depending on the technique used, figure 5) is understandable. They further point out that the use of a single technique over a limited range of Reynolds numbers could give misleading results.

There is insufficient data in the literature concerning Reynolds number effects at other Mach numbers. Regarding the effect of Mach number available data show an increase in the pressure rise to IS (or equivalently α_{is}) with M_o which is to be expected on general grounds and is consistent with the free interaction principle.

The turbulent separation process being intermittent in character, the difficulties associated with locating IS experimentally can be reconciled with since different techniques would average the unsteady nature of the flow in a different manner.

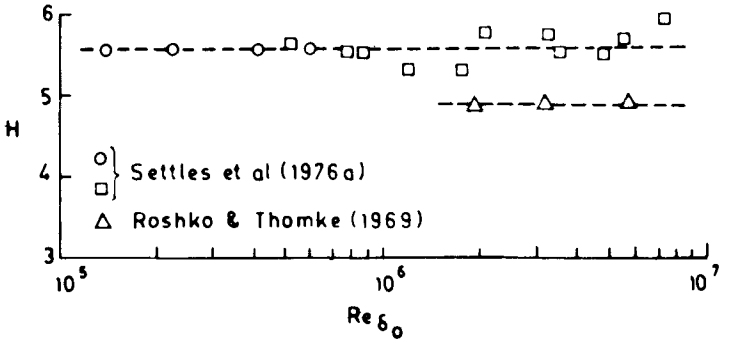

Figure 6. Shape factor variation with Reynolds number at M_o = 3·0.

Although information on mean properties is sufficient from an engineering or practical view point, further understanding of the IS process and the effects of Reynolds number may require deeper understanding and modelling of the unsteady character of the turbulent separation process described earlier (§ 3.2). Perhaps there is need to reexamine the concept of IS in view of the unsteady nature of the turbulent separation phenomena.

4. Supersonic interactions: Fully separated flows

Progressive increase in the shock strength or overall pressure rise beyond incipient separation leads to rapid thickening of the subsonic stream tubes and a corresponding increased deflection of the supersonic part of the boundary layer. As a result, the adverse pressure gradient in the interaction region increases leading to significant deceleration of the flow near the wall. The boundary layer near the wall eventually separates when it can no longer negotiate the pressure gradients imposed by the outer inviscid flow. Boundary layer separation leads to a bubble of reversed flow followed by reattachment. Further increase in the overall pressure rise following separation generally causes a further increase in the separated zone.

4.1 *Some general features*

In figure 7 are shown some schematic representations of the wave pattern and surface pressure distributions, for three different interactions, due to impingement of a shock on a flat wall, in front of a compression corner and a forward facing step. Wall pressures are shown for both laminar and turbulent cases to bring out qualitatively some of the major differences. The separation and reattachment of the boundary layer are indicated by S and R respectively. The pressure distributions for the compression corner and the incident shock have much in

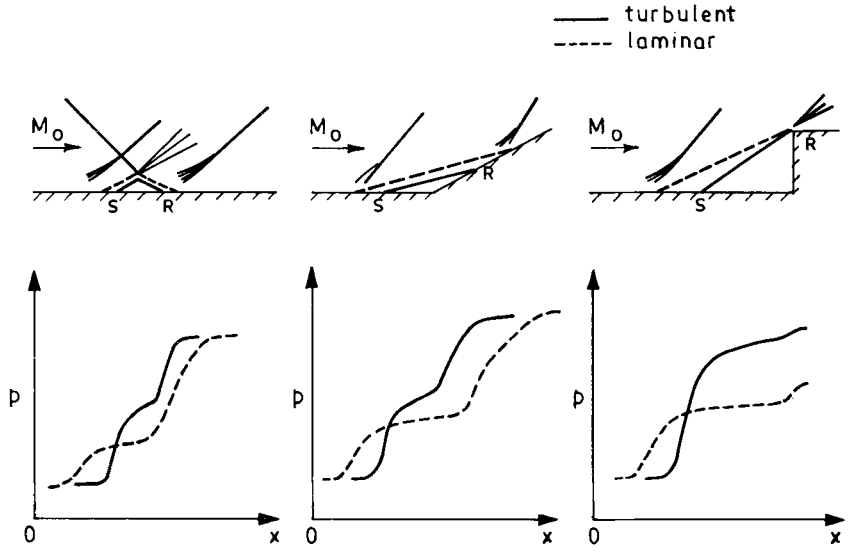

Figure 7. Schematic of wave pattern and wall pressure distributions in supersonic separated flows.

common; three distinct regions, pressure rise due to separation, a reduced or zero pressure gradient in the bubble region and pressure rise following reattachment may be observed. The separated boundary layer grows as a free shear layer which acquires kinetic energy as a result of mixing and is able to overcome the pressure gradient at reattachment. For the interactions at a forward facing step, the reattachment occurs on the step face and the separation location is free to move. In the vicinity of separation the pressure distribution is similar to the two cases just described earlier, while downstream, it looks somewhat different.

For laminar separated flows the pressure rise to separation and the pressure gradients, in general, are relatively smaller than for the corresponding turbulent case; furthermore, the interaction spreads over a longer streamwise distance for the same overall pressure rise.

4.2 *Free interaction concept*

The basic mechanism that causes boundary layer separation involves a two-way localized interaction between the boundary layer flow and the inviscid outer supersonic flow. Based on an extensive series of experiments on various experimental configurations, Chapman *et al* (1957) postulated the concept of "free interaction." They suggested that, if the separated region is large enough, the interaction in the vicinity of separation is localized, free of downstream influences (or geometry) and independent of the agency provoking separation. In essence, the separation process would depend only on the Mach number and the boundary layer characteristics ahead of the interaction.

Chapman *et al* (1957) used simple order of magnitude analysis to derive expressions for similarity in pressure distributions in the separation region. For supersonic flow under small rate of boundary layer growth, the local pressure coefficient may be related to the growth of the displacement thickness:

$$c_p = (p - p_o)/q_o = [2/(M^2 - 1)^{1/2}]\,(\mathrm{d}\delta^*/\mathrm{d}x), \tag{1}$$

where o refers to conditions at the beginning of the interaction. For viscous flow, boundary layer approximations are assumed valid; the momentum equation applied at the wall gives

$$\mathrm{d}p/\mathrm{d}x = (\partial\tau/\partial y)_w. \tag{2}$$

Equation (2) emphasizes the importance of the flow near the wall for analysing separation.

Applying order of magnitude considerations and introducing a length scale l_f (characteristic of the free interaction region), (1) & (2) can be written as

$$(p - p_o)/q_o \sim [1/(M^2 - 1)^{1/2}](\delta^*/l_f), \tag{3}$$

$$(p - p_o)/l_f \sim \tau_{wo}/\delta^*. \tag{4}$$

Algebraic manipulation of (3) and (4) leads to

$$(p - p_o)/q_o \sim (c_{fo})^{1/2}/(M_o^2 - 1)^{1/4}, \tag{5}$$

$$l_f/\delta_o^* \sim 1/[(c_{fo})^{1/2}(M_o^2 - 1)^{1/4}]. \tag{6}$$

These expressions are valid for both laminar and turbulent interactions provided

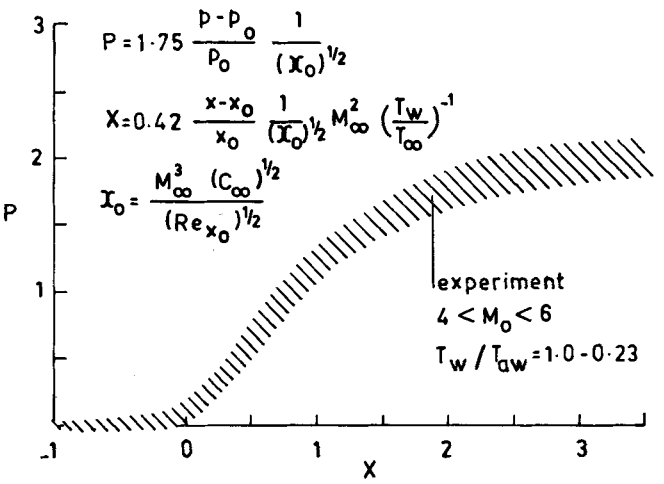

Figure 8. Free interaction similarity in laminar flow (from Lewis 1967).

appropriate $c_f \sim \mathrm{Re}_x$ relationships are chosen. Good correlation of experimental data at moderate Reynolds numbers were seen (Chapman *et al* 1957) in the expressions suggested above.

Extensions and refinements of the free interaction concept have been reported in the literature; two such examples are shown in figures 8 and 9. Pressure

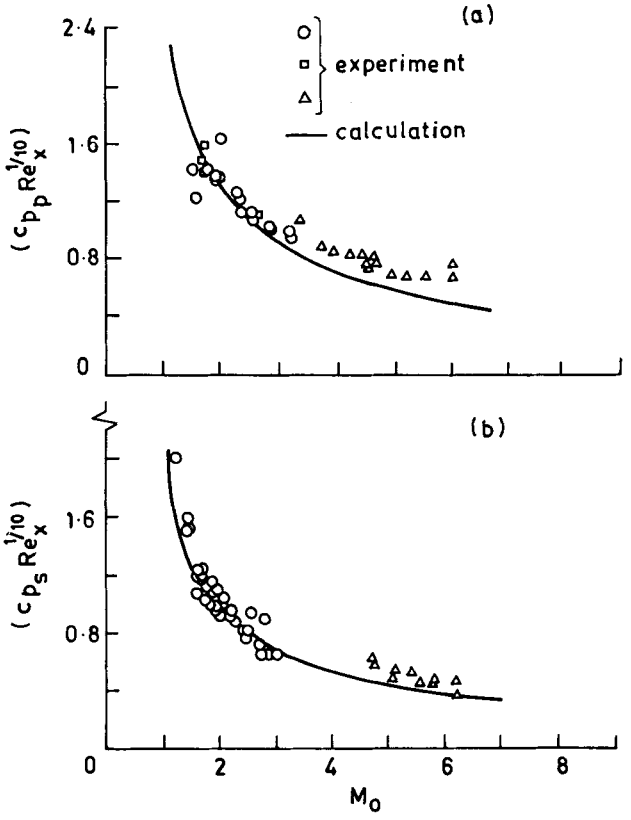

Figure 9. Free interaction similarity in turbulent flow (from Erdos & Pallone 1962), (a) plateau pressure rise, (b) separation pressure rise.

distributions, in the variables suggested (Lewis 1967), are shown in figure 8 for laminar-separated flow at a compression corner at different values of M_o and Re including effects of surface heat transfer. Good correlation may be seen for the separation including the plateau region although the similarity parameters are expected to be valid only for the free interaction region in the vicinity of separation. For the turbulent case, results of separation and plateau pressure rise are shown in figure 9 from the semi-empirical theory of Erdos & Pallone (1962, pp. 239–254). Reasonably good agreement may be seen except for some departure at the higher M_o for the plateau pressure rise, which has been attributed to the linearized expression used in describing the inviscid flow. With turbulent interactions, unlike the laminar counterpart, similarity in pressure distributions (for different geometries) are not clearly observed (Chapman *et al* 1957) beyond the separation point, indicating relatively stronger influence of the downstream geometry.

4.3 *Flow development through the interaction*

Although a large number of experimental investigations with separated flows have been reported, the flow-field has been explored only in very few of these. Certain broad features of separated flows were discussed in the previous sections. Both surface and flow-field data are now discussed based on the measurements of Settles *et al* (1976b) on a 24° compression corner at a Mach number of 2·85 and at high Reynolds number.

Distributions of surface pressure and skin friction (obtained using a Preston tube) distributions are displayed in figure 10. The pressure distribution shown is

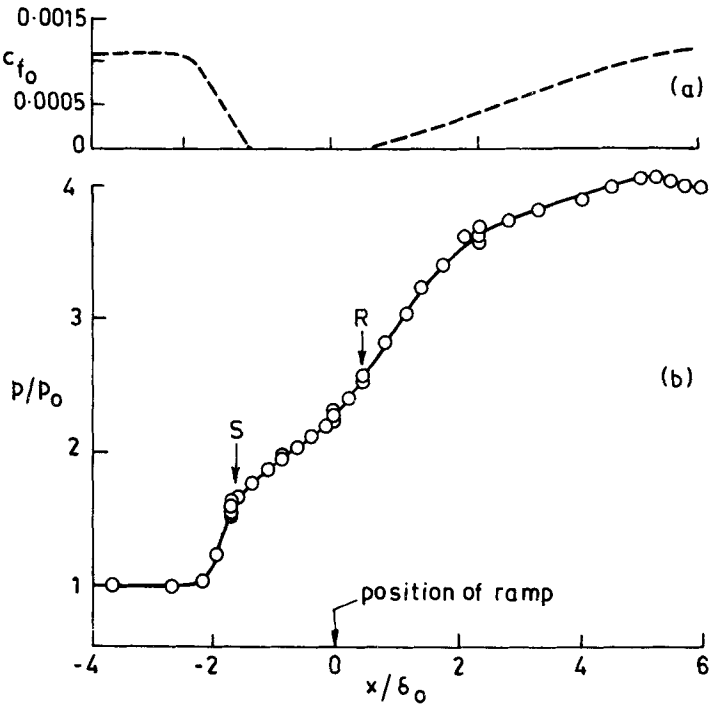

Figure 10. Experimental data for a compression corner flow: $M_\infty = 2{\cdot}9$ (from Settles *et al* 1976b), (**a**) skin friction distribution (**b**) wall pressure distribution.

typical of compression-corner-separated flows. The c_f distributions show a rapid decrease towards separation and a more gradual recovery following reattachment. Both surface oil flow technique and c_f data reveal a bubble length of about 2 δ_o. The pressure gradients in the bubble region suggests that they are apparently balanced by the Reynolds stress gradients, since the velocities in the reversed flow are small. The maximum reversed flow velocity was only about 15% of the boundary layer edge velocity in these experiments.

Development of streamwise mean velocity profiles through the interaction is shown in figure 11. Significant retardation of the flow, particularly near the wall in the separated zone, is evident. Static pressure measurements in this flow have revealed significant normal pressure gradients near separation and reattachment, arising out of streamline curvature. Gross features of the flow-field determined from detailed measurements are shown in figure 12. The separation shock-wave originates at a distance of about 2 δ_o upstream of the corner turning the outer flow by 10°. The sonic line is displaced outwards considerably as a result of flow separation. A system of compression waves is generated in the reattachment zone which coalesce with the separation shock.

With flow separation, turbulence quantities in general undergo significant variations through the interaction. At supersonic speeds, detailed information on turbulence quantities like kinetic energy and shear stress does not exist as yet for shock separated flows. There are, however, some data available in the absence of separation (Rose 1973; Rose & Johnson 1975) which show effects which are typical of adverse pressure gradient flows. A discussion of turbulence behaviour for a shock separated flow at transonic speeds is included in § 5.4.

4.4 *Scaling of upstream influence interaction length*

It is of considerable interest to determine scaling laws for different characteristic lengths associated with the separated flow. Figure 13 shows suitably defined lengths characterizing separation, reattachment and bubble size for fully separated flows;

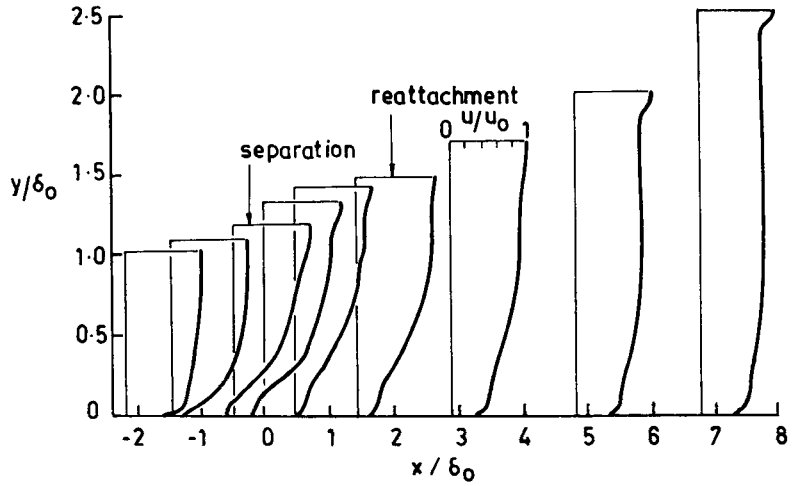

Figure 11. Mean velocity profiles in the interaction region: M_o = 2.9 (from Settles *et al* 1976b).

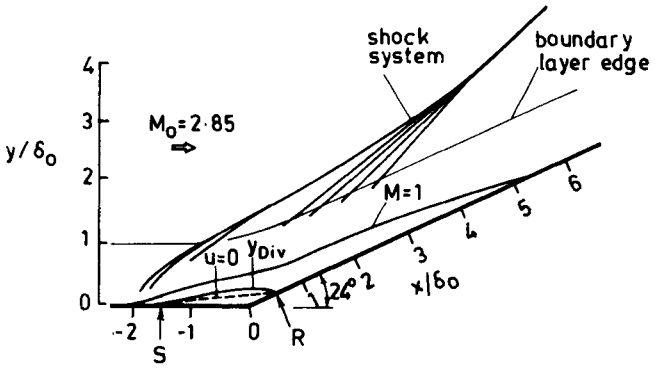

Figure 12. Features of separated flow at a compression corner: M_o = 2.9 (from Settles *et al* 1976b).

these lengths can be determined without much difficulty from experimental pressure distributions. In the literature, however, several attempts have been made to determine the scaling for the interaction length, l_o, associated with the upstream influence phenomena (figure 13). The boundary layer thickness, δ_o, at the beginning of the interaction has been used for normalising l_o in most earlier studies. We shall now present two correlations that have been proposed in the context of compression corner flows.

The free interaction principle provides a frame work for analysing and correlating experimental data, in particular, to characterize certain gross features of the separated flow as they depend on important variables like M_o, Re etc. Doubts have often been raised as to the validity of these arguments at higher Reynolds numbers, an example of which was seen in connection with the experimentally determined pressure rise to incipient separation (figure 5).

For boundary layers developing on a flat plate ahead of interaction, in general, we may expect l_o/δ_o, to depend on M_o, Re_{δ_o}, and the ramp angle α. Results l_o/δ_o from different experiments at relatively higher Reynolds numbers show (e.g. Roshko & Thomke 1969, pp. 109–138) the following general trend; it decreases with increase in M_o (for fixed values of Re_{δ_o} and α) and Re_{δ_o} (for fixed values of M_o

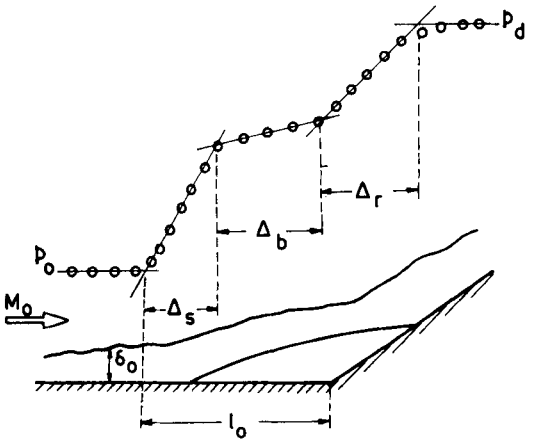

Figure 13. Sketch defining characteristic lengths in separated flow.

and α); it increases with α for given values of M_o and Re_{δ_o}. These results may imply an increased resistance to separation with increase in Re_{δ_o} and M_o.

Roshko & Thomke (1976), based on an extensive series of tests in the range $2 < M_o < 4{\cdot}5$ and $10^5 < Re_{\delta_o} < 10^6$, found that, for $M_o > 2$, their data l_o/δ_o correlated with c_{fo} at each ramp angle independent of both M_o and Re_{δ_o} (figure 14). Other data from the experiments of Law (1974) and Settles *et al* (1976a), at relatively high Reynolds numbers, were found to be in good agreement with the above correlation. The physical reasoning behind this correlation is not known; the trend of these results with Reynolds number is in clear contradiction with the free interaction principle.

The second correlation is due to Settles & Bogdonoff (1982) and is based on simple dimensional arguments; for a compression corner, one can write

$$l_o/\delta_o = f(M_o,\ Re_{\delta_o},\ \alpha).$$

Figure 15 shows their data at $M_o = 3$ as well as those of Law (1974) and Roshko & Thomke (1969, pp. 109–138); at each α, l_o/δ_o decreases with Re_{δ_o}. They obtain, after choosing an average value of $-1/3$ for the slope,

$$(l_o/\delta_o)(Re_{\delta_o})^{1/3} = 0{\cdot}9\exp(0{\cdot}23\alpha), \text{ at } M_o = 3{\cdot}0.$$

To throw further light on these observations, Settles & Bogdonoff (1982), based on their measurements at $M_o = 3$, examined the variation of other relevant boundary layer length scales (e.g. displacement, and momentum thicknesses, distance to sonic line, sub-layer thickness) with Re_{δ_o}; none of these exhibited the $Re_{\delta_o}^{-1/3}$ variation suggested by the correlation.

In conclusion, while engineering correlations for an interaction length associated with separation are now available for compression corner flows over limited M_o and Re_{δ_o} ranges, our understanding of the influence of the Reynolds number, particularly at the higher range of practical interest is rather poor. A similar

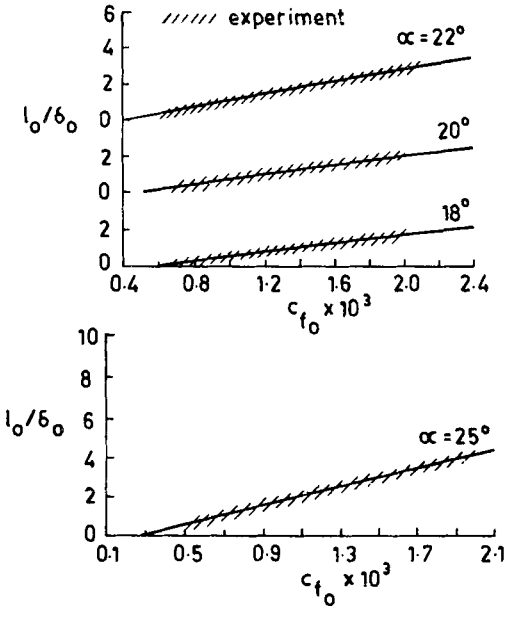

Figure 14. Correlation of interaction length at a compression corner (from Roshko & Thomke 1976).

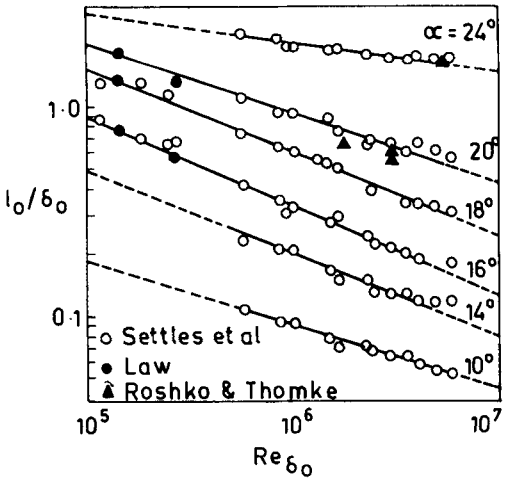

Figure 15. Variation of interaction length with Reynolds number at a compression corner: $M_\infty = 2.9$ (from Settles *et al* 1982).

situation can be expected with other interactions also (e.g. impinging shock wave, forward facing step etc); sufficient data covering a wide range of Re does not even exist for these cases to attempt such a correlation. It is therefore not surprising that little information exists for the scale of the separation bubble or the reattachment region (figure 13); even identifying relevant parameters for these cases may not be easy.

4.5 *Certain experimental aspects*

Experimental research has provided the most valuable information on the subject of shock-wave-boundary-layer interaction. Two aspects of experimental testing which have proved to be very important are now discussed.

4.5a *Three-dimensional effects in nominally two-dimensional interactions*: To realize nominally 2D interaction in experiments is a difficult task, particularly in the presence of strong adverse pressure gradients. Differences in the experimental results amongst experiments conducted in different tunnels on similar geometrical configurations and in similar flow conditions, have often been due to varying degrees of three-dimensional (3D) effects. It is very important to make as many checks as possible to assess departure from two-dimensionality or the degree of 3D effects in any experiment. 3D effects arise largely from shock-boundary layer interactions on the side wall when the model spans the wind tunnel side walls. Isolating the central part of the model flow by some means or use of side fences are known to minimize 3D effects (Settles *et al* 1976b). Use of axisymmetric geometry is a good remedy, but would require a model of a larger size so that the transverse curvature effects are reduced to a minimum; furthermore, large size of the model would imply a larger size for the wind tunnel. Another source of error could arise if the scale of separation (e.g. extent of separated zone) becomes comparable to the span of the tunnel, which is in essence an aspect ratio effect.

Various methods are available for assessing the degree of two-dimensionality. The surface oil flow technique is widely employed to assess the spanwise uniformity of the surface flow and to locate the separation-reattachment points; it has been a

very valuable tool in separated flow experiments. An assessment of spanwise variation of flow or surface parameters would be very useful. The 2D boundary layer momentum balance through the interaction region should be assessed; this exercise would involve measurements of streamwise mean velocity profiles and surface parameters like skin friction and pressures.

Every attempt should be made to keep the 3D effects to a minimum in experiments. This is important from the point of view of understanding the true behaviour of the flow, for providing quality data for validating calculation methods and for providing the necessary feedback to the modeller.

4.5b *Tripping device and occurrence of transition*: An assessment of the state of the boundary layer ahead of the interaction is an important requirement since the interaction, in general, is strongly dependent on the nature of the boundary layer. Most experiments reported in the literature have been conducted in relatively small tunnels which imply smaller models; this combined with the stagnation pressure supply generally available have lead to insufficiently high Reynolds numbers in which natural transition can occur well ahead of the interaction. Therefore the boundary layer is often tripped downstream of the leading edge of the model to ensure a turbulent boundary layer ahead of the interaction; the presence of the trip also avoids varying transition locations at different Reynolds numbers. Having tripped, checks have rarely been made to assess the state of the boundary layer. It is well-known that tripping becomes more difficult at relatively lower Reynolds numbers and higher Mach numbers because of the increased stability of the laminar boundary layers.

It has often been argued (e.g. Green 1970, pp. 235–340) that, in experiments conducted in tunnels at relatively low Reynolds numbers with a tripping device, the boundary layer upstream of the interaction may not have been fully developed or close to equilibrium. This effect may have contributed to another source of error while comparing different sets of data on similar configurations and flow conditions. Realizing their importance, boundary layer velocity profile measurements have been made ahead of the interaction in many recent studies. In some of the experiments (e.g. Settles *et al* 1976b) care has been taken to ensure that the boundary layer exhibits the well-known law of the wall and wake regions.

5. Transonic interactions

5.1 *Some general features*

Normal shock-wave-boundary-layer interactions occur in a variety of flow situations; on airfoils at transonic speeds, in supersonic intakes, in supersonic nozzles/diffusers etc. Interactions at transonic Mach numbers, in general, have not received much attention; the renewed interest in transonics after 1970 has triggered many new investigations in the last decade. Transonic-shock-boundary-layer interactions exhibit certain features distinct from those at supersonic speeds, as illustrated by the following two examples.

The first is the interaction between a normal shock wave and a flat plate boundary layer, studied by several investigators (Seddon 1960; Kooi 1975; Sawyer *et*

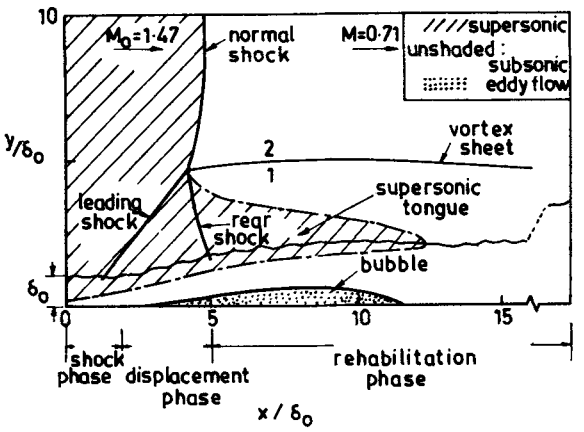

Figure 16. Interaction of normal shock with a turbulent boundary layer: M_o = 1.47 (from Seddon 1960).

al 1977). Figures 16 and 17 show some of the important features of the separated flow and the surface pressure distributions as observed by Seddon (1960). The strong normal shock wave bifurcates near the wall (leading to what is often called lambda shock) as a result of flow separation; the leading shock results from free interaction between the boundary layer flow and the outer inviscid flow. Behind the rear shock there is a supersonic region, often referred to as a supersonic tongue, which generally occurs for $M_o \gtrsim 1{\cdot}40$. Because of the differences in the static pressures and flow directions in regions 1 and 2 of figure 16 a vortex sheet or slip line originates at the lambda intersection. The downstream flow is subsonic, hence, downstream conditions can exert significant effects on the entire interaction. The surface pressure increases continuously in the interaction zone towards the inviscid value and the distribution in general does not exhibit a plateau region like in supersonic interactions at relatively higher Mach numbers. The overall total pressure rise through the interaction is, in general, decided by the strong interaction between the viscous flow and the outer inviscid flow and is not known a priori. In view of the fairly extensive region of separation, and because of the influence of the downstream subsonic flow, interactions at transonic speeds are relatively less localized, adding further to the difficulty in prediction of these flows.

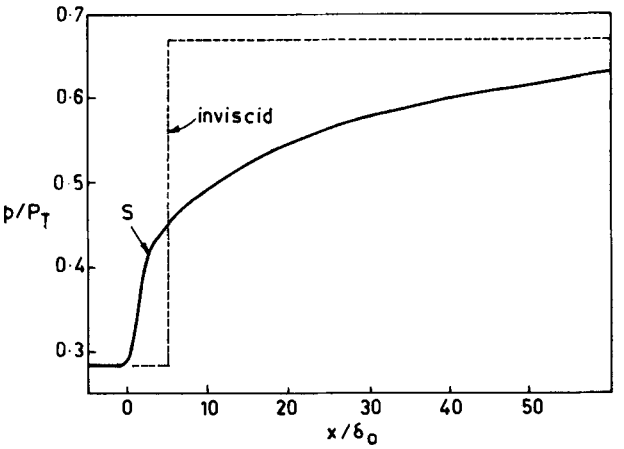

Figure 17. Surface pressure distribution due to normal-shock-turbulent-boundary layer interaction: M_o = 1.47 (from Seddon 1960).

The second example illustrates additional complexity that can arise if the separated shear layer does not reattach to a surface, as often happens on an airfoil (figure 18). The flow is seen to separate at the foot of the shock wave and leaves downstream a massive separated flow. Two main differences relative to flat plate interactions may be observed here. The boundary layer upstream of the shock interaction develops in a region of continuous favourable pressure gradient caused by the airfoil contour; depending on the shock strength and the airfoil geometry, the separated shear layer may close only in the wake downstream of the airfoil trailing edge (figure 18), adding further complexity to the modelling of the reattachment process.

5.2 *Unseparated flows*

Figure 19 shows a sketch of a normal shock wave interaction for which the boundary layer does not separate ($M_o \leq 1{\cdot}30$). The flow downstream of the shock

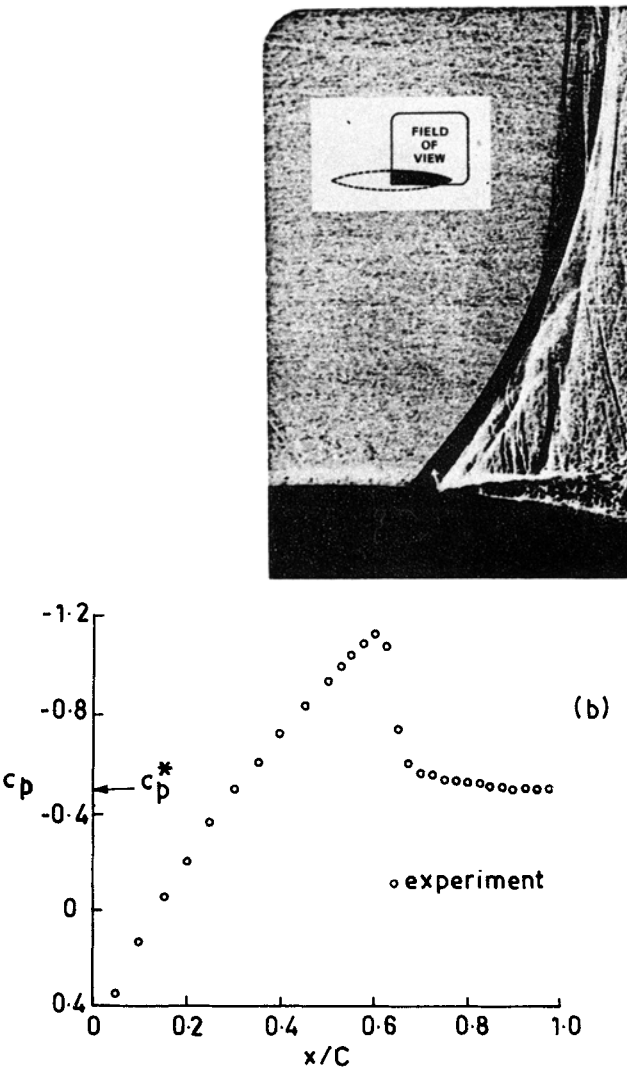

Figure 18. Shock-induced separated flow on a circular arc airfoil: $M_\infty = 0.78$ (from McDevitt 1979), (**a**) shadowgraph of the flow-field, (**b**) surface pressure distribution.

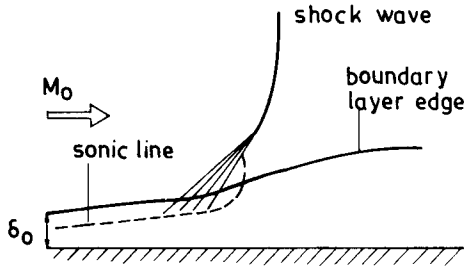

Figure 19. Schematic of wave pattern due to normal shock-turbulent boundary layer interaction (from Melnik & Grossman 1974).

is subsonic and the interaction is not localized in contrast to the supersonic case. Thickening of the subsonic stream tubes, as a result of upstream influence, generates compression waves at the foot of the shock wave. The subsonic part of the boundary layer, having a large fraction of the boundary layer thickness, plays an important role in the generation of the wave system. The boundary layer thickness increases across the interaction.

5.3 *Incipient separation*

Very few investigations have dealt with the problem of incipient separation at transonic Mach numbers. The difficulties in experimentally determining incipient separation discussed in connection with supersonic interactions are present in the transonic case also. Experimental results (Delery 1985) obtained by different techniques are shown in a plot of M_o vs. Re_{δ_o} (or H_{io}) in figure 20. The shape factor has only a weak influence in determining incipient separation; a slight rise in M_o at low values of H_{io} is indicated, which is consistent with fuller velocity profiles associated with low values of the shape parameter. Inger's (1981) result based on a triple deck analysis shows (figure 20) fair agreement with the data.

Certain important features of the flow just following incipient separation, taken from the experiments of Delery (1983), are shown in figures 21 and 22. Measurements were made in the interaction zone at the diverging end of a symmetric nozzle at $M_l = 1{\cdot}30$. The mean velocity profiles, as a result of the adverse pressure gradients imposed by the shock, go through a significant deceleration particularly near the wall (stations 2, 3); following the pressure gradient relief beyond station 4, the velocity profiles recover again near the wall.

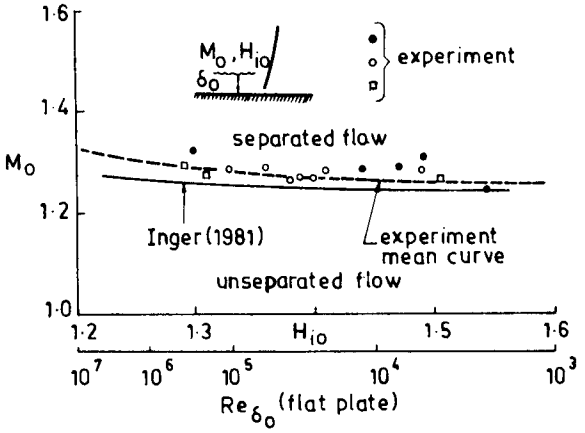

Figure 20. Experimental data of shock-induced incipient separation in transonic flow (from Delery 1985).

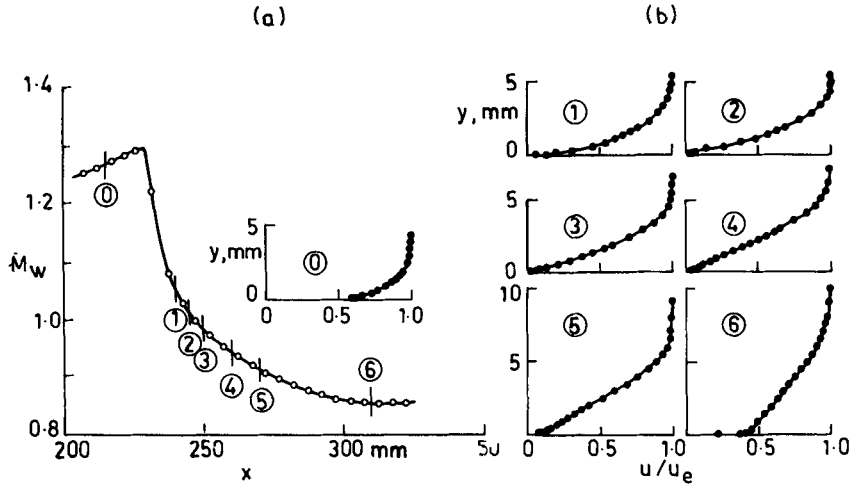

Figure 21. Experimental data at nearly incipient separation condition (from Delery 1983), (**a**) wall Mach number distribution, (**b**) mean velocity profiles.

location; following the relief in the pressure gradients, H_i decreases and returns to the flat plate value downstream. The streamwise velocity intermittency data (described in § 3.2), measured using a laser velocimeter, are shown in figure 22, in terms of the probability for the instantaneous value of U, to be negative, i.e. $P(U \leq 0)$, which corresponds to $(1-\gamma_p)$. These measurements reveal a tiny bubble about 2 δ_o in streamwise length. The intermittent flow reversal near the wall is spread over a distance of about 2 δ_o upstream of the mean separation point.

5.4 *Fully separated flows*

Experimental results indicate (figure 20) that the turbulent boundary layer at transonic speeds separates for $M_I \gtrsim 1{\cdot}30$; with a fully separated flow, dissipative phenomena play a major role in determining the dynamics of the mean flow. There have been, in recent years, quite a few experimental investigations (Delery 1981; Bachalo & Johnson 1979) wherein the flow-field with separation has been

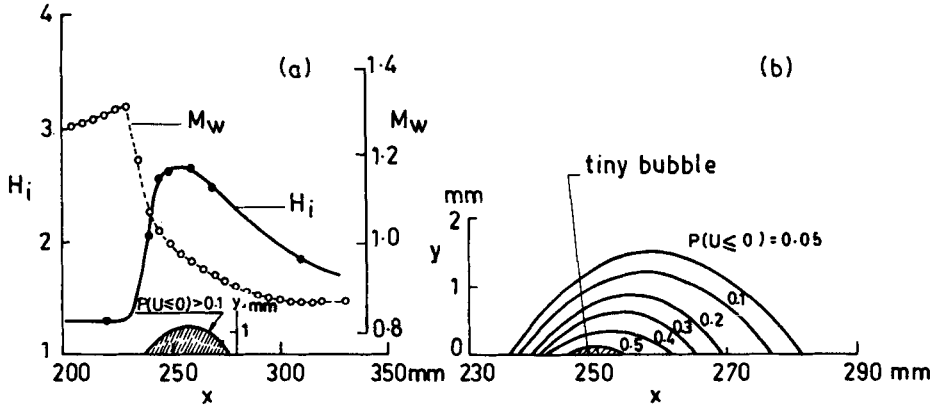

Figure 22. Experimental data at nearly incipient separation condition (from Delery 1983), (**a**) shape factor and wall Mach number distributions, (**b**) lines of constant value for $P(U \leq 0)$.

have been, in recent years, quite a few experimental investigations (Delery 1981; Bachalo & Johnson 1979) wherein the flow-field with separation has been explored. The flow development through such an interaction will be discussed based on results obtained by Delery (1983) on a bump in a transonic channel.

Figure 23 shows the wall Mach number distributions and an interferogram of the flow-field. The shock interaction occurs at $M_l = 1{\cdot}37$; a well-defined separated flow results and reattachment occurs on the flat wall downstream of the bump trailing-edge. The Mach number distributions suggest a pressure plateau in the bubble zone followed by a pressure rise associated with the shear layer reattachment.

Results of mean velocity and turbulent quantities measured with a laser anemometer are shown in figures 24 to 26. The mean velocities are shown normalized with respect to boundary layer edge values; the turbulent kinetic energy and shear stress data are normalized by the stagnation speed of sound so that absolute changes across the interaction can be clearly seen. In the separated zone, maximum reverse flow velocities reach about 20% of local boundary layer edge

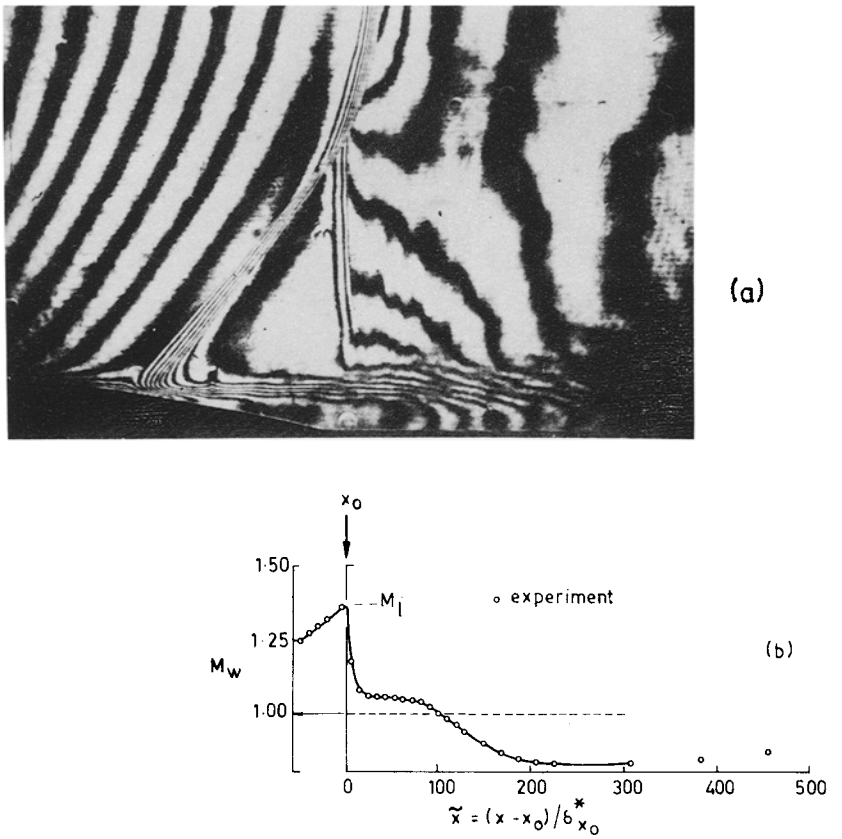

Figure 23. Shock-induced separated flow on a bump: $M_l = 1{\cdot}37$ (from Delery 1981), (**a**) interferogram of the flow-field, (**b**) wall Mach number distribution.

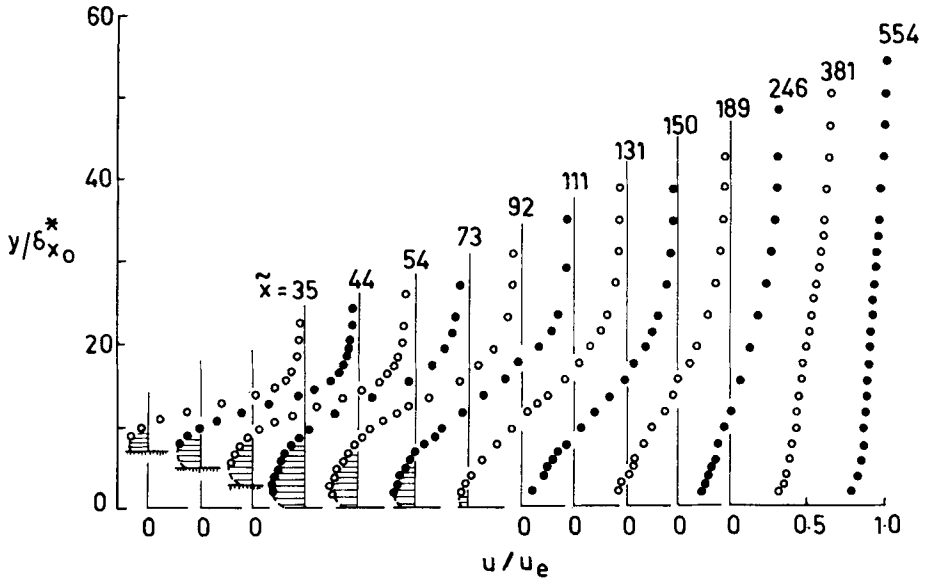

Figure 24. Mean velocity profiles in the interaction region: $M_l = 1.37$ (from Delery 1983).

velocities and the vertical extent of the bubble is as large as about 10 times the value of δ^* at the beginning of interaction. The velocity profiles, otherwise, are qualitatively similar to what one would find in low speed separated flow.

The turbulent kinetic energy and shear stress profiles show streamwise variations which are qualitatively similar. Following the start of the separation process, both kinetic energy and shear stress levels increase rapidly with streamwise distance. These profiles, in the separated region, exhibit clear maxima in the neighbourhood

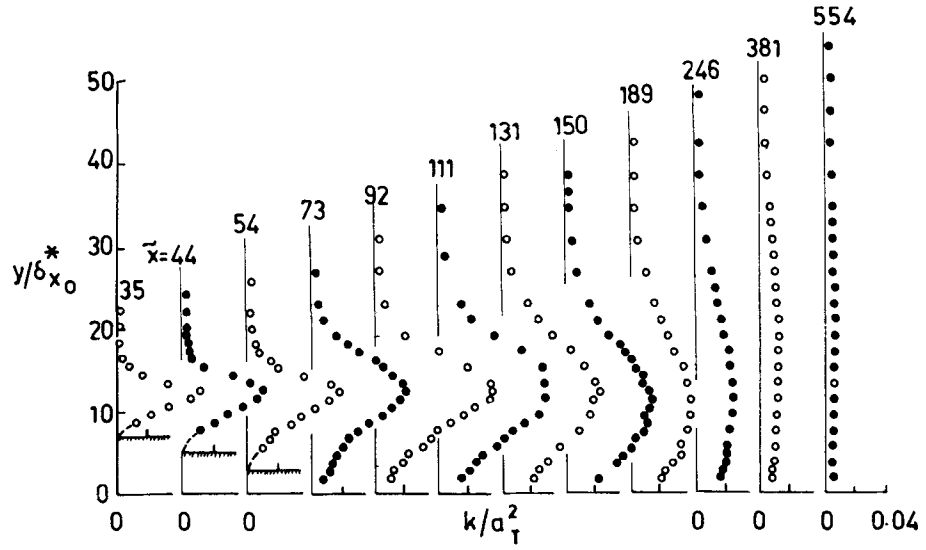

Figure 25. Turbulent kinetic energy profiles in the interaction region: $M_l = 1.37$ (from Delery 1983).

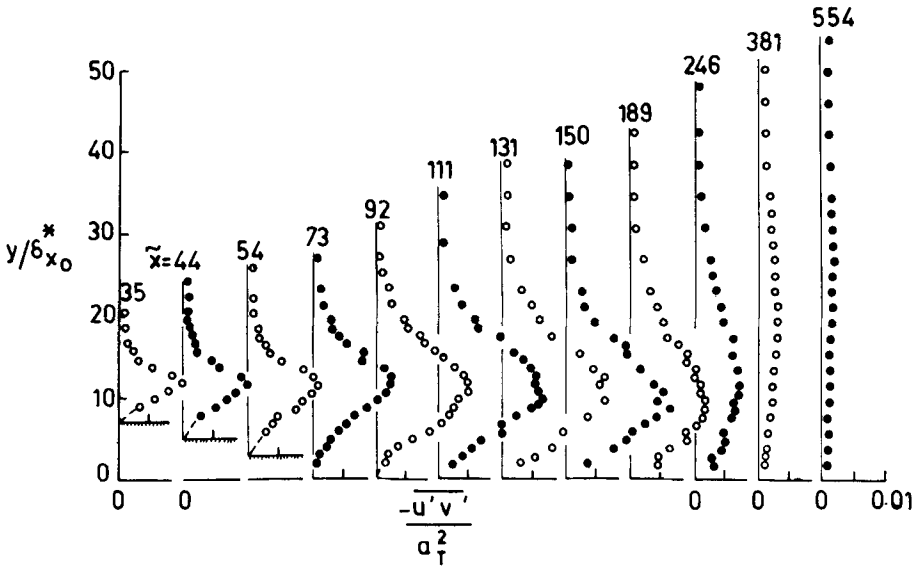

Figure 26. Turbulent shear stress profiles in the interaction region: $M_l = 1.37$ (from Delery 1983).

of the maximum mean velocity gradient, $\partial u/\partial y$ (well away from the wall). Data on streamwise evolution of the maximum kinetic energy and shear stress (figure 27) show that they reach peak values well downstream of separation and rather close to the reattachment location. Following reattachment, these peak values diminish gradually as the flow develops into a new equilibrium state.

Analysis of turbulence data has revealed (Delery 1983) that (i) the turbulent normal stress term assumes importance in the vicinity of separation, both from the point of view of mean flow dynamics as well as in the production of turbulence energy; and (ii) that the turbulent shear flow, as a result of flow separation, undergoes significant departures from equilibrium (see figure 42 on p. 181). Following separation, there is a significant lag in the turbulent shear stress. Downstream of reattachment, the relaxation towards a new equilibrium state is a rather long process due to the memory of the large scale structures. These results suggest the strong need for one or more transport equations for modelling turbulence in these complex interactions.

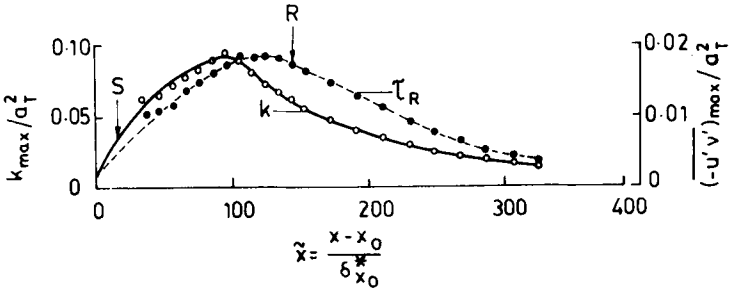

Figure 27. Maximum turbulent shear stress and kinetic energy variation in the streamwise direction: $M_l = 1.37$ (from Delery 1983).

In addition to modelling history effects, there appears to be a need to account for the direct effects of shock waves on turbulence. The analysis of Anyiwo & Bushnell (1982) combined with available experimental information has shown that shock waves can amplify turbulence in the shear layer through three major mechanisms: (i) direct amplification of incident turbulence across a shock region, (ii) generation of turbulence from incident acoustic and entropy fluctuations, and (iii) conversion of mean flow energy into turbulence by shock oscillations. Their results, based on linear analysis, show that amplifications by as much as 100% of the incident turbulence intensity are possible across shocked regions. They suggest that these effects could be a significant factor in the observed large increase in the turbulent shear stress and kinetic energy across the shock in regions of separation. In the absence of a shock wave, for example, at low speeds one would normally expect a frozen or nearly frozen Reynolds stress behaviour along streamlines in regions of rapidly varying pressure gradients as a result of rapid distortion of turbulence (e.g. Narasimha & Sreenivasan 1973; Narasimha & Prabhu 1972).

5.5 *Interaction length*

Since, in general, transonic shock-boundary layer interactions involve both supersonic and subsonic regions in the outer inviscid part of the flow, one can expect more difficulty in trying to correlate experimental data. The attempts, therefore, have been to look for a correlation for a suitably defined "interaction length" for the supersonic domain of the interaction, and in the absence of separation (Sirieix *et al* 1981, pp. 149–214).

Figure 28 shows a typical interferogram and wall Mach number distribution at $M_o = 1{\cdot}3$ (Sirieix *et al* 1981, pp. 149–214). Domain I is characterized by rapid supersonic compression to a local Mach number of 1·0 and domain II primarily involves gradual subsonic diffusion depending on downstream conditions, shape of the wall etc.

As in supersonic interactions, the primary variables include the Mach number M_o ahead of the shock, a characteristic Reynolds number Re, the overall shock pressure rise and a boundary layer shape parameter to take into account (in a gross manner) the pressure gradient effects, if any, upstream of the interaction. However the pressure rise itself depends on M_o, Re and model geometry. For domain I, M_o can be taken to represent the pressure rise.

In figure 29 is shown l^*/δ_o^* vs. M_o with $\mathrm{Re}_{\delta_o^*}$ as a parameter for a fixed value of H_{io}, the incompressible shape parameter; figure 29 shows significant effects of H_{io} for fixed M_o. The boundary layer displacement thickness δ_o^* appears to be a useful normalizing factor, which takes into account the effect of Re. The correlation suggests that the extent of interaction decreases with increase in $\mathrm{Re}_{\delta_o^*}$. The weak dependence of M_o (for a fixed value of H_{io}) seems surprising (figure 29) since an increase in l^* with M_o (or equivalently shock pressure rise) is to be expected; perhaps this increase is compensated by the decreased upstream influence arising out of the thinning of the sonic layer for a fixed value of H_{io}. A correlation for the transonic 'supersonic interaction length', based on data obtained from different facilities and different states of the boundary layer ahead of interaction, has been suggested by Sirieix *et al* (1981, pp. 149–214); the empirical law is of the form

$$l^*/\delta_o^* \simeq 70\ (H_{io}-1).$$

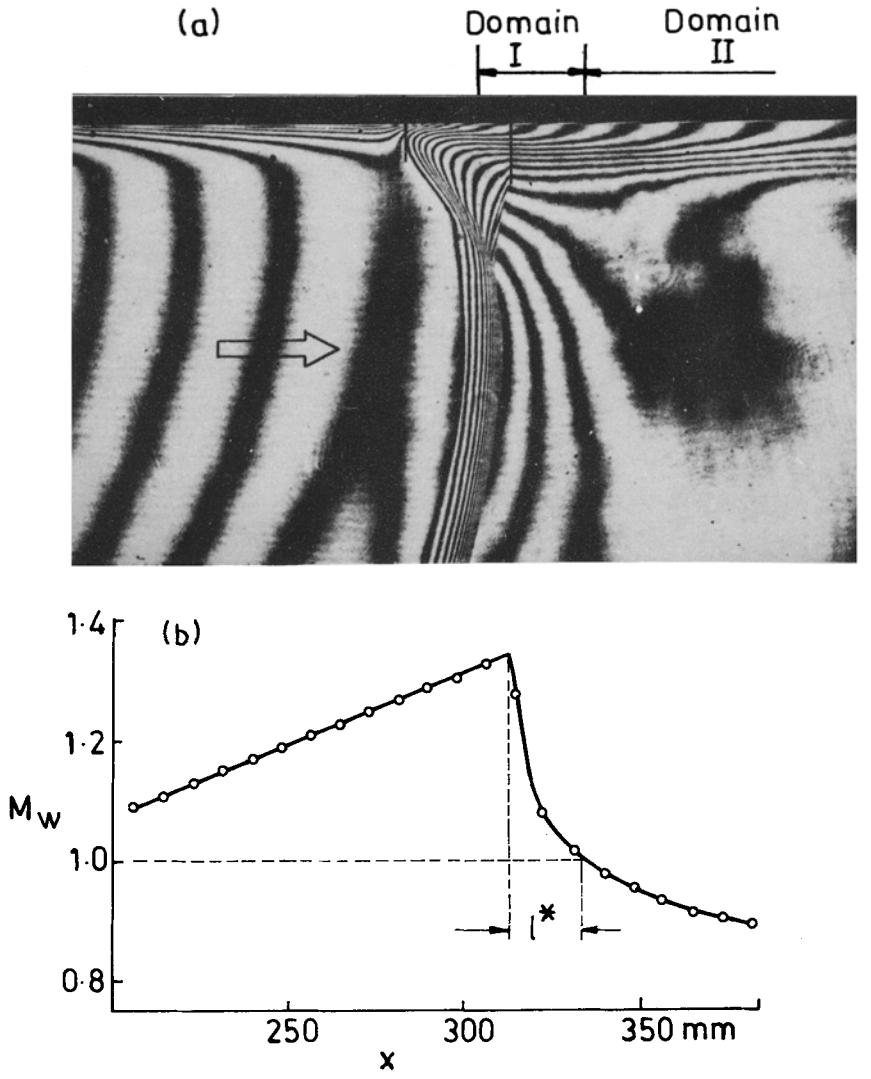

Figure 28. Definition of interaction length in transonic interaction (from Sirieix *et al* 1981). (**a**) interferogram of the flow-field, (**b**) wall Mach number distribution.

With flow separation, a simple picture is unlikely to result for reasons indicated earlier. Results presented by Kooi (1980) for the length of the separation bubble as a function of Re_{δ_2} with M_∞ as a parameter are shown in figure 30; these data refer to boundary layer interactions on a flat plate obtained in different facilities. Although there is some scatter in the data (which may be due to effects of three-dimensionality, different techniques used for defining separation bubble etc), a strong dependence on both M_∞ and Re_{δ_2} is quite evident as in the case of supersonic interactions. There appears to be insufficient data to examine if there is any systematic effect of the shape parameter on the non-dimensional bubble length.

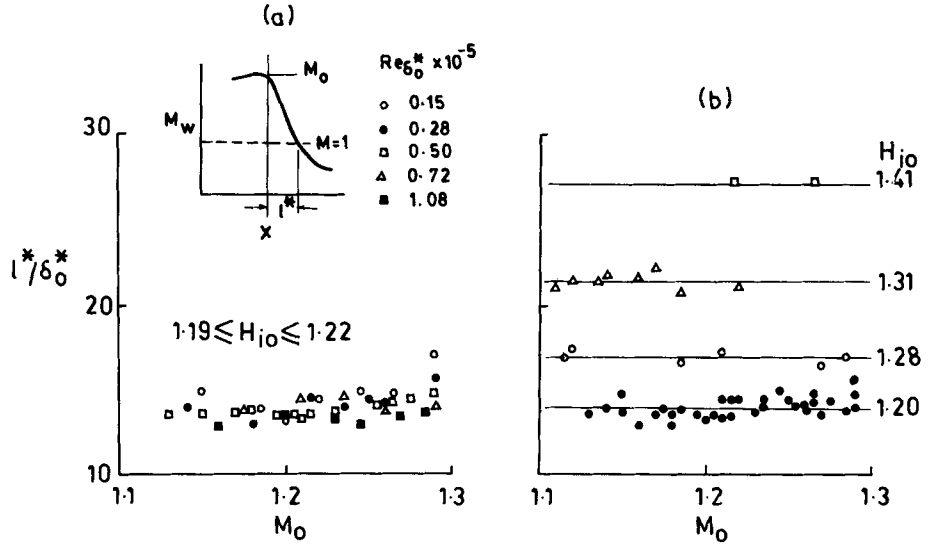

Figure 29. Data of interaction length in transonic interaction (from Sirieix *et al* 1981), (a) effect of Reynolds number (b) effect of incompressible shape factor.

6. Certain unsteady features of shock wave-turbulent boundary layer interactions

An important unsteady feature of a turbulent separating flow, namely its intermittent character of separation, was briefly touched upon in § 3.2. There are several examples in the literature (Kistler 1964; Eaton & Johnston 1982, pp. 162–170; Dolling & Murphy 1983; Driver *et al* 1983) indicating that, even when the mean flow approaching separation is nominally steady, turbulent separated flows often have in them some gross or large scale unsteadiness (e.g. oscillation of the bubble, oscillations of separation and reattachment points, excursion of a shock wave). A basic question is whether such low frequency unsteadiness is an inseparable

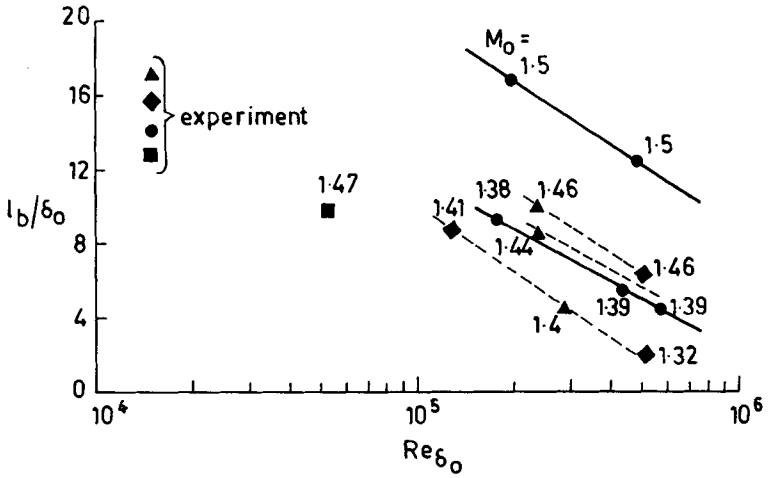

Figure 30. Variation of bubble length with Reynolds number (from Kooi 1980).

ingredient of all turbulent separated flows, and if so, how important it is in modelling mean flow dynamics. In the literature, not much attention has been paid to this modelling aspect.

There is now growing evidence (e.g. Dolling & Or 1983) that the shock wave, when it interacts with a turbulent boundary layer, is generally unsteady even in the absence of separation; the shock oscillations or excursions appear to be driven by turbulence in the shear flow (Plotkin 1975; Grande & Oates 1973). These oscillations can amplify turbulence (Anyiwo & Bushnell 1982) in the flow thereby adding another element of complexity in the turbulence modelling of these interactions. Two examples of the unsteady character of shock-separated flows at supersonic speeds, as revealed by surface measurements, are briefly discussed.

Unsteady surface pressure fluctuations obtained by Dolling & Murphy (1983) for a separated compression corner flow at $M_o = 2{\cdot}9$ (discussed in § 4.3) are displayed in figure 31. A large peak upstream of separation and a second (weak) peak close to reattachment in the r.m.s. values may be seen; these are presumably a result of the unsteady shock wave structure in the vicinity of separation and reattachment. Pressure-time history of the signals just upstream of separation displayed in figure 32 shows strong intermittent character of the wall pressure – jumping back and forth in a random fashion between a low level characteristic of the undisturbed boundary layer to a higher level that varies with the instantaneous shock position and strength. Similar features have also been observed by Kistler (1964) in a separated flow induced by a forward facing step at $M_o = 4{\cdot}0$. Presumably the mean wall pressure is generated by the superposition of these relatively low frequency large amplitude fluctuations on the undisturbed wall pressure. An intermittency factor, suitably defined to represent the fraction of the time the wall pressure is disturbed (upstream of separation) from its undisturbed value, shows (Dolling & Murphy 1983) that it reaches a value of 1·0 near the location of the peak r.m.s. value (figure 31); shock excursion is assessed to be of the order of δ_o based on these measurements. These measurements also show that the extent of upstream influence continuously varies with time. Power spectral measurements in the intermittent and in the separated zone show (e.g. Dolling & Or 1983; Coe *et al* 1973) that there is an enormous increase (at least a factor of 100) in the power

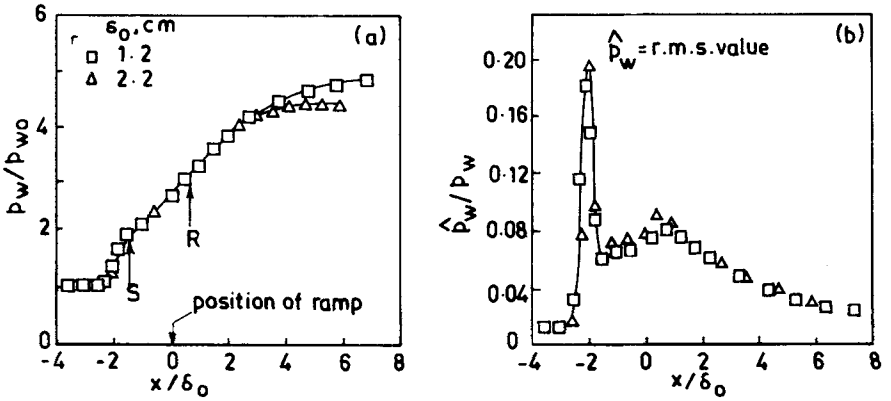

Figure 31. Wall pressure distributions in a compression corner separated flow (from Dolling & Murphy 1983), (**a**) mean value, (**b**) r.m.s. value.

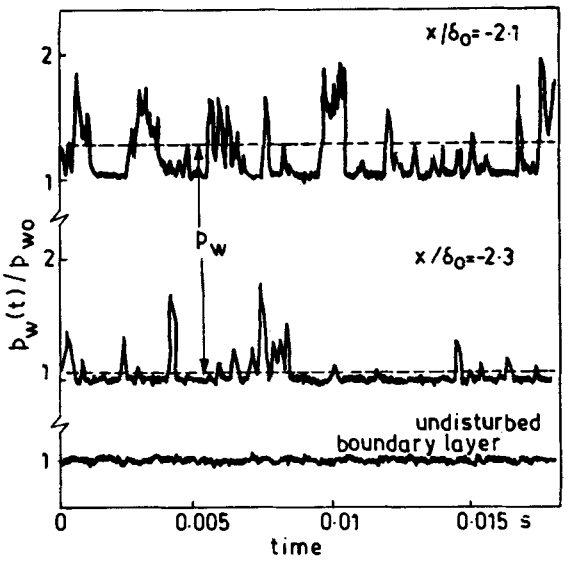

Figure 32. Pressure-time histories near separation (from Dolling & Murphy 1983).

levels at relatively low reduced frequencies in comparison with the attached boundary layer flow upstream.

Observations of separated flow unsteadiness in hypersonic (impinging) shock-wave-turbulent-boundary layer interactions (Horstman & Owen 1974) on an

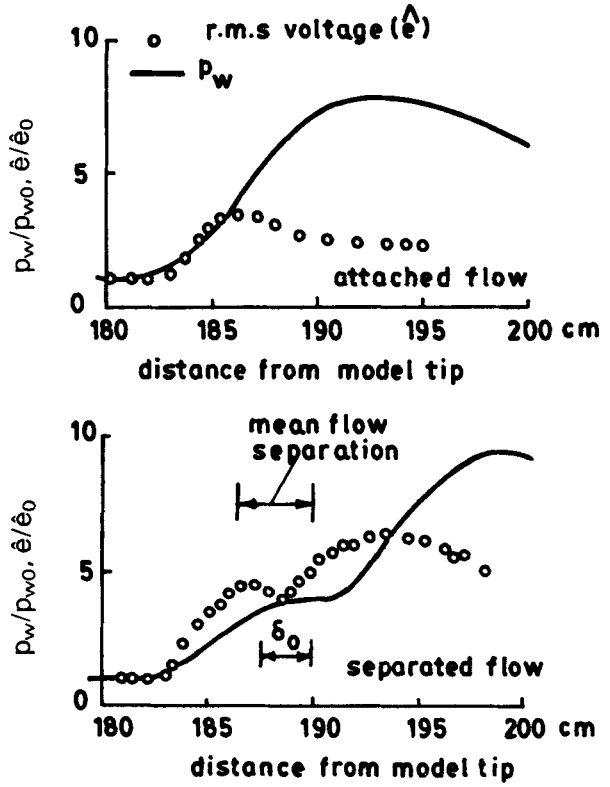

Figure 33. Distribution of mean surface pressure and r.m.s. voltage from thin-film gauge (from Horstman & Owen 1974).

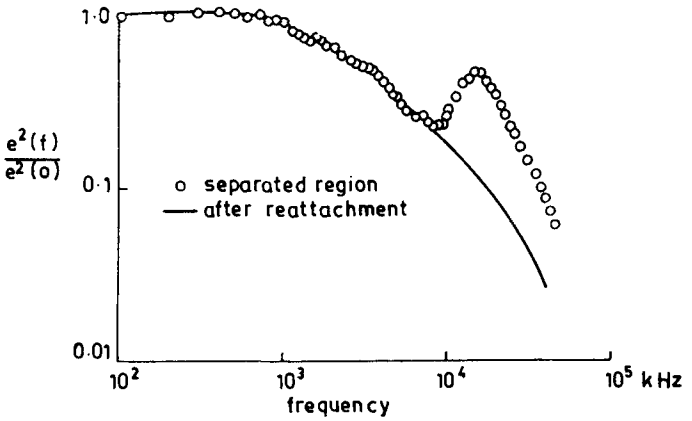

Figure 34. Normalised energy spectra in the interaction zone (from Horstman & Owen 1974).

axisymmetric model are shown in figures 33 and 34. Normalized r.m.s. voltages measured by a surface mounted heated thin film gauge (figure 33) indicate significant increases in r.m.s. values upstream of separation and just downstream of reattachment, which are broadly similar to those of the compression corner flows discussed earlier (figure 31). The normalized power spectra in the separated region reveal (figure 34) a pronounced periodicity around a frequency of 15 kHz ($f\delta_o/u_o \simeq 0{\cdot}5$); such a peak was not observed either in the upstream attached turbulent boundary layer or in laminar separated flow on the same model at lower Reynolds numbers. These suggest an oscillatory nature of the separated flow which is confirmed by correlation measurements as well. What causes this observed periodicity is not known; there is insufficient information in literature to judge if the periodicity is peculiar to separated flows caused by impinging shock waves. The length scale of unsteadiness for this flow was found to be of the order of the streamwise extent of the separated zone (figure 33).

In transonic flows, although the frequent occurrence of such unsteadiness has been known for a long time [for example, in wind tunnels (Liepmann 1947; Meier 1975), on airfoils (Finke 1975) and in supersonic intakes (Seddon & Goldsmith 1985)], detailed information on the unsteady aspect of shock interactions even for simple geometries (e.g. on a flat plate) seems absent. Since normal shock-boundary layer interactions often involve massive separation, unsteady effects in transonic interactions may be even more severe and important than at higher speeds. Investigations of unsteady features in connection with normal shock-boundary layer interactions would be of considerable interest, both from the point of view of basic fluid mechanics as well as in practical applications.

7. Calculation methods for shock wave-boundary layer interaction

The last fifteen years have seen considerable development in the ability to calculate both laminar and turbulent separated flows. This has been made possible by the rapid developments in computer speed and memory and parallel advances in the

development of efficient numerical algorithms for solving the equations governing fluid motion. Progress has also been made in the asymptotic description of laminar supersonic free interactions and turbulent interactions in the transonic regime in the absence of separation. In this section, following a brief presentation of results obtained from asymptotic methods, we shall highlight features of viscous-inviscid interaction methods and Navier-Stokes methods, and then show results from state-of-art calculations and comparison with experiments. Approximate/semi-empirical calculation methods, which are useful for design purposes, are omitted from the discussion here; examples of these may be found in the publications by Green (1970) and Stanewsky (1973).

7.1 *Asymptotic theories*

Results from asymptotic theories provide considerable insight with regard to the dominant physical mechanisms operating in the different regions of flow, and provide appropriate scaling laws. In general, they can also be very useful for assessing the accuracy of numerical schemes since they become more reliable at higher Reynolds numbers where numerical computations become more difficult.

Asymptotic theories, valid for $\mathrm{Re} \to \infty$, are now fairly well developed for the analysis of laminar free interactions in supersonic/hypersonic flows. These are based on the original ideas of Lighthill (1953) and have been developed further in detail by Neiland (1969), Messiter (1970) and Stewartson & Williams (1969). These theories indicate that as $\mathrm{Re} \to \infty$, solutions of the Navier-Stokes equations develop a multi-layered structure widely referred to as the "triple-deck". Applications of the asymptotic theory to various problems have been summarized by Stewartson (1974). Adamson & Messiter (1980) have presented a comprehensive survey of the investigations employing asymptotic techniques to shock wave-boundary layer interaction problems. Asymptotic flow structures for two problems are described in the following paragraphs.

7.1a *Laminar flow past a compression corner*: An example of triple-deck structure that develops in front of a compression corner in supersonic laminar flow (Burggraf *et al* 1979) is shown in figure 35. If the ramp angle α^* is of order $\mathrm{Re}^{-1/4}$, separation first occurs and a triple-deck structure develops with a longitudinal length scale of the disturbed region of order $\mathrm{Re}^{-3/8}$ centred about the plate compression corner junction; with further increase in α, separation moves upstream and a well-defined plateau region forms between separation and reattachment (Burggraf 1975).

In the interaction region, there are three distinct scalings in which different physical mechanisms dominate. The middle (or main) deck has a transverse scale of

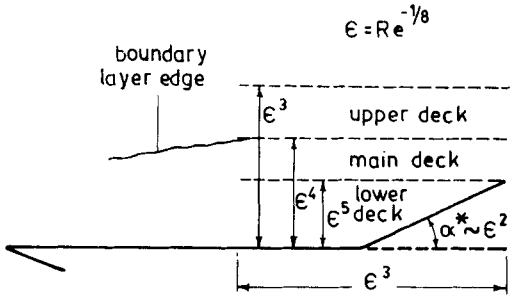

Figure 35. Asymptotic flow structure at a compression corner (from Burggraf *et al* 1979).

$Re^{-1/2}$ and is simply the streamwise continuation of the upstream boundary layer. Since the interaction region is short, the dominant mechanism is an inviscid turning of streamlines in the upstream boundary layer. The lower deck is characterized by viscous flow essentially to satisfy the no-slip condition at the wall; this deck has a traverse length scale of order $Re^{-5/8}$ and is governed by classical boundary layer equations. Because the wall layer is very thin, flow here is essentially incompressible. The boundary conditions involve the no-slip condition at the wall and a new edge condition which results from the matching of the inviscid rotational middle deck. The flow in the lower deck responds strongly to the compressive disturbances producing large vertical motions which displace the main deck outwards, which in turn displaces the upper deck. The upper deck has a transverse length scale of order $Re^{-3/8}$ and consists of fluid which is disturbed by the flow in the interaction region through the outward propagation of Mach waves. The flow in the upper deck is inviscid and irrotational.

The mathematical problem has been dealt with in detail by Stewartson (1974) and by Rizetta *et al* (1978). Approximate analytical as well as numerical solutions have been obtained for the shock interaction problems (e.g. Stewartson 1974, Rizetta *et al* 1978, Burggraf *et al* 1979). Comparisons of pressure distribution predicted from triple-deck analysis (Rizetta *et al* 1978) and experiments (Lewis *et al* 1968) are shown in figure 36 for a 10° ramp at $M_\infty = 4{\cdot}0$ and $Re_L = 68{,}000$. The triple-deck result, while giving a good qualitative trend, is seen to overpredict the upstream pressure rise. It is of course to be remembered that the triple-deck solution is only valid in the limit $Re \to \infty$.

7.1b *Normal-shock-turbulent-boundary-layer interactions at transonic speeds*: Weak shock interactions with a turbulent boundary layer developing on a flat plate have been analysed by several investigators (e.g. Melnik & Grossman 1974; Adamson & Feo 1975); all these analyses correspond to interactions without separation. Basic features of these interactions, as revealed by the studies of Melnik & Grossman (1974, 1975, pp. 262–272, 1977, pp. 415–433) are described next.

In the transonic case, two basic parameters appear in the problem, namely, the Mach number ahead of the interaction and the Reynolds number. The analysis involves asymptotic expansion of the Reynolds-averaged Navier-Stokes equations in the double limit $M_\infty \to 1$ and $Re \to \infty$. The Reynolds number parameter is expressed in terms of a non-dimensional frictional velocity, $E = u_*/U_\infty$, so that the solution is obtained in the double limit $M_\infty \to 1$ and $E \to 0$. Melnik & Grossman

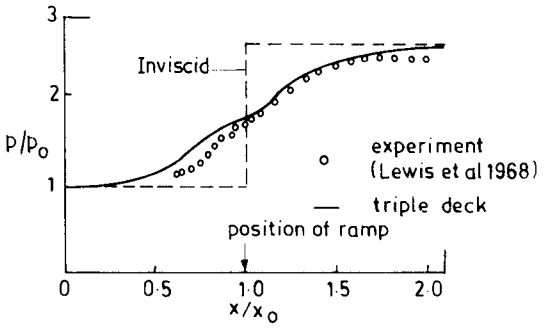

Figure 36. Comparison of predicted surface pressure distribution with experiment (from Rizetta *et al* 1978).

(1974) define a parameter $X_t = (M_\infty^2 - 1)/E$ which controls the relative rates at which the two parameters M_∞ and E approach their respective limits. Two distinguished limits, corresponding to weak and strong shocks, respectively, were considered.

The main features of the interaction problem and the asymptotic flow structure corresponding to the weak shock limit, $X_t = 0(1)$, are shown in figure 37. In the regions upstream and downstream of the interaction zone, the flow exhibits the conventional turbulent-boundary-laver-inviscid-flow structure, with the former having the well-known law of the wall/law of the wake structure. In the shock-interaction zone, the boundary layer develops a three-layer structure: (1) an outer layer (or main deck) extending over most of the boundary layer which is inviscid but rotational, (2) a wall layer which is a continuation of the upstream wall layer in which the total shear stress (laminar plus turbulent) is constant across it; and (3) a blending (or Reynolds stress) layer coupling the inner and outer layers. In the outer layer the Reynolds stresses are nearly frozen because of the short streamwise scale of the interaction zone. In the inner layer, on the other hand, Reynolds stresses are in equilibrium with the local skin friction, which varies in the streamwise direction. The mismatch in the Reynolds stresses across the outer and inner layers is resolved by the blending layer solution; in this layer there is a balance between the inertia, the pressure gradient and the Reynolds stress terms. The derivation of the governing equations and the boundary and matching conditions are contained in the papers cited above. Fairly good agreement of

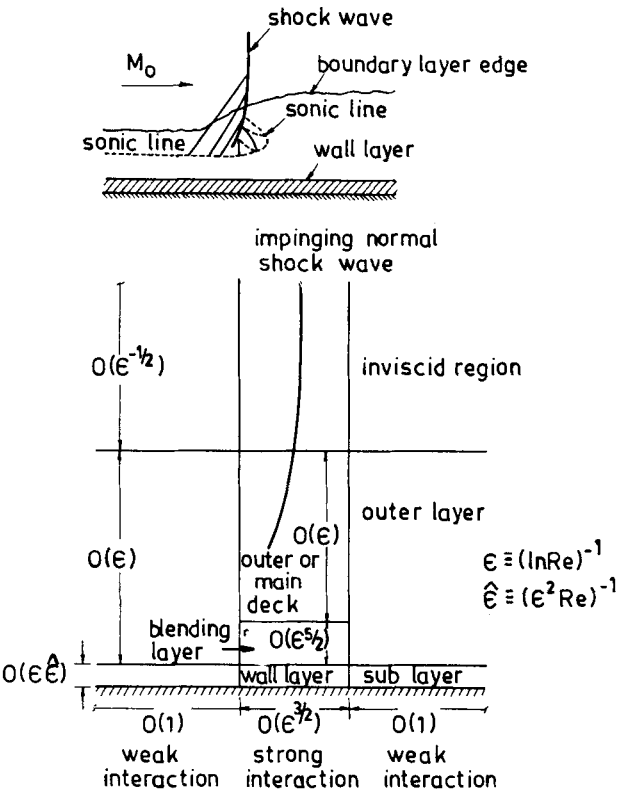

Figure 37. Asymptotic flow structure for a weak normal shock wave-boundary layer interaction (from Melnik & Grossman 1974, 1975).

theoretical wall pressure distributions was obtained with Gadd's (1961) experimental data obtained in an axisymmetric internal flow.

It is of interest to note some of the similarities and differences between the laminar and turbulent interactions. In both, the major part of the boundary layer flow is governed by inviscid equations. A four-layer structure in the interaction zone appears for a turbulent boundary layer, in contrast with a three-layer structure for laminar flows; this is because the former has a two layer structure as opposed to a single layer structure in laminar flows. For laminar flows, the growth of the viscous layer has strong effects on the main deck and the outer flow, and solutions for all three layers have to be determined simultaneously. This is in contrast to a turbulent weak interaction, wherein, to a first approximation, the wall layer does not influence the outer layer and the inviscid flow. This is because the wall layer in which flow deceleration takes place is much thinner (a fraction of $\delta_{,,}$) than in the corresponding laminar flow. This feature allows calculation of wall pressure distributions without taking into account the wall layer in turbulent interactions. These results would of course become inaccurate once separation sets in. There are examples in the literature (Roshko & Thomke 1969, pp. 109–138; Elfstrom 1972) to show that, for unseparated turbulent interactions at supersonic/hypersonic speeds, the surface pressure distributions calculated ignoring the sub-layer are in good agreement with experimental data. The results from the asymptotic analyses also suggest that the choice of a turbulence model could influence the wall skin friction distributions, but may only have a weak effect on prediction of surface pressures. Numerical calculations of Viegas & Horstman (1978) for shock interactions in an axisymmetric internal flow support these findings.

To summarize, for turbulent interactions with a shock wave, asymptotic methods have been applied to steady, two-dimensional attached flow situations at transonic speeds; approximate theories based on the two-layer hypothesis of Lighthill (1953) have also been reported (Inger & Mason 1976); an example of such a calculation was seen in figure 20. With boundary layer separation, complications arise from reversed flow zones, normal pressure gradients and turbulence closure problems.

7.2 *Viscous-inviscid interaction methods*

The term "viscous-inviscid interaction" refers to all flow situations wherein the viscous flow in the boundary layer has noticeable influence on the pressure distribution. In 'weak' interactions the viscous effects on the potential flow pressure distributions are generally small; viscous effects on an airfoil in subcritical flow without separation is an example. On the other hand, for example, in the vicinity of unseparated shock-boundary layer interaction and in the separation-reattachment regions of a separated flow, viscous effects are significant and the interaction is generally termed 'strong' because of the strong coupling between the viscous and inviscid parts of the flow field. Calculations of turbulent interactions therefore involve modelling both strong viscous-inviscid interactions as well as turbulence in the shear layers.

Considerable progress has been made in the development of very sophisticated viscous-inviscid interactive methods. Although there are many differences in the details of these methods, the three main elements of such a method are:

(i) a technique for obtaining a solution of the inviscid part of the flow-field; in principle, any inviscid flow "solver" can be used;

(ii) a method for obtaining a solution for the viscous boundary layer flow (with flow separation, special treatment is necessary);

(iii) a coupling equation to link the inviscid and viscous flow solutions at a suitable location in the flow, and an efficient iterative scheme providing convergence of the interactive calculations.

A variety of procedures is now available for solving both potential as well as Euler equations. With regard to items (ii) and (iii) mentioned above, some further discussion seems appropriate.

7.2a *Viscous flow solution*: There is now growing evidence (Cebeci *et al* 1984, pp. 1–40; McDonald & Briley 1984, pp. 141–162) that boundary layer approximations are useful and adequate for analysing flows with small separated zones. Favourable comparisons of boundary layer solutions (used in an interactive calculation) with triple-deck and Navier-Stokes results for laminar flow problems are now available (e.g. Rizetta *et al* 1978; Burggarf *et al* 1979). However, in the solution of the boundary layer equations, two problems arise when applied to flows involving separation. The first is the classical Goldstein singularity at separation which arises when the pressure distribution $p(x)$ is prescribed; the second involves difficulties associated with the appearance of reverse flow velocities following separation. The singularity can be avoided by specifying not $p(x)$ but rather an interaction law between the viscous and inviscid flows, as suggested by Crocco & Lees (1952). Solving the boundary layer equations in an "inverse mode" also eliminates the separation singularity. In the inverse mode, the classical outer boundary condition, $\lim_{y\to\infty} u(x, y) = u_e(x)$, is replaced by prescribing a displacement thickness distribution $\delta^*(x)$, or a wall skin friction distribution $c_f(x)$, which must be satisfied by the solution; the pressure gradient $p(x)$ [or $u_e(x)$] comes out as part of the solution. The problem associated with the reversed flow arises because of the forward marching along the flow into the separated region. Several numerical schemes have been devised to overcome this difficulty (e.g. Klineberg & Steger 1974, Carter 1975). Interesting discussions on the use of boundary layer equations in interactive calculations may be seen in the paper by McDonald & Briley (1984, pp. 141–162).

Integral methods have been favoured in most interactive methods primarily because of their simplicity and ability to give good engineering predictions when properly tailored. It seems much easier to incorporate empirical information into such methods than into finite difference calculations. First-order boundary layer equations are generally adopted in the derivation of the momentum integral equations, although some of the recent methods (e.g. La Balleur & Blaise 1985) include an allowance for non-zero pressure variation across the boundary layer. In addition to the momentum integral equation, additional auxiliary equations, for example the mean kinetic energy equation or an equation for entrainment, are used.

Certain closure relationships including modelling turbulent shear stresses are generally necessary before the complete set of equations can be solved. These involve specification of (i) relationships among boundary layer integral thicknesses and shape parameters, (ii) a skin friction law, and (iii) information required to evaluate the entrainment equation or dissipation integral etc. For the calculation of

separated flows, it is also important to model the nonequilibrium or history effects, which is done through the use of a lag equation in calculating the entrainment or the dissipative integral. Simplified turbulent transport integral equations may also be employed for determining the lag effects.

More details on some of the integral techniques currently used in connection with interactive methods may be seen in the publications by La Balleur (1981), Lock (1981) and Whitfield *et al* (1981).

7.2b *Viscous-inviscid coupling*: The coupling algorithm relating the viscous and inviscid parts of the flow-field plays a crucial role in the successful calculation of these complex flows. Considerable attention has been paid to the mathematical and numerical aspects of these coupling techniques (e.g. La Balleur 1984, pp. 259–284, Carter 1985, Veldman 1984, pp. 343–363). Three schemes which have been frequently employed are shown in figure 38.

7.3 *Navier-Stokes calculation methods*

In this approach, mean flow solutions of the "Reynolds-averaged" Navier-Stokes equations (RANS) are obtained numerically. The approach has an inherent advantage since the viscous-inviscid interactions are naturally built into the equations, so that the potential exists for assessing turbulence modelling aspects in a systematic manner.

Rapid advances have been made in the development of efficient algorithms for solving RANS. Notable amongst these are the methods of McCormack (1976, 1982) and Beam & Warming (1978). The equations are parabolic in time and elliptic in space, and are solved numerically in time until steady-state solutions are reached. Surveys of various methods in use have been presented by McCormack & Lomax (1979) and Mehta & Lomax (1982).

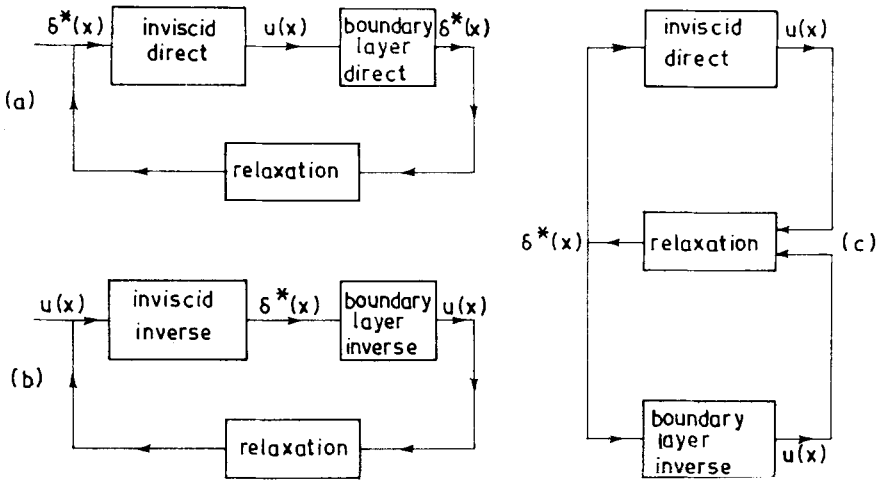

Figure 38. Calculation schemes used in viscous-inviscid interactive methods: (**a**) direct, (**b**) inverse, and (**c**) semi-inverse.

7.3a *Turbulence modelling aspects*: In the RANS, the turbulent stresses have to be modelled to close the system of equations governing the fluid motion. Furthermore, in compressible flow applications, the product of density and velocity fluctuations that appears in the equations of mean motion also needs to be modelled. To overcome this difficulty, mass-averaging (or Favre-averaging) of the governing equations is employed which reduces the equations to the incompressible form. For a further discussion of compressibility effects in turbulence modelling, the reader is referred to the paper by Rubesin (1982).

The models that have been used may be classified as either eddy viscosity or Reynolds stress models. In the former the Reynolds stresses are assumed proportional to the mean strain rate or velocity gradient. The resulting eddy viscosity is a property of the flow-field and can be looked upon as being proportional to the product of a velocity and the length scale of turbulence. These models may be further classified under zero-, one-, and two-equation models which refer to the additional partial differential equations employed to define the eddy viscosity.

The zero equation model represents an equilibrium model in which the eddy viscosity is related algebraically to the mean-flow variables. The Cebeci-Smith model is a typical example of this type. The one-equation model uses an additional partial differential equation for the turbulent kinetic energy which defines the velocity scale for determining the eddy viscosity; the length scale is prescribed by an algebraic equation. Glushko's (1965) model is a typical example of this type. In the two-equation models, two partial differential equations, one for the turbulent kinetic energy and the other for obtaining a length scale, are solved to define the eddy viscosity function. The Jones-Launder (1971) and Wilcox-Rubesin (1980) two-equation models have been used with RANS for shock separated flows. The one- and two-equation models do account for history effects to some degree since turbulent transport equations are utilized in arriving at the eddy viscosity. The specification of boundary conditions for turbulent properties is an added requirement with these models; the studies of Cebeci & Meier (1979) suggest that the uncertainties introduced by the boundary conditions may not be small. Finally, it may also be noted that all these models have been primarily developed for incompressible unseparated boundary layer flows.

In Reynolds stress models, all the equations for the relevant Reynolds stresses are modelled and are free of the assumption that the stresses respond immediately to change in mean strain rate. The difficulties in modelling at this level have led to approximate methods (e.g. Bradshaw *et al* 1967). These models may also utilize additional differential equations for either the length scale or rate of dissipation. There appears to be hardly any attempt in which stress modelling is used for computing shock-boundary layer interactions.

Excellent discussions of turbulence modelling aspects for high speed separated flows may be seen in the papers by Marvin (1982, 1983) and Viegas & Horstman (1978).

7.4 *Computations and comparisons with experiments*

In this section, examples of state-of-art calculations from both interactive methods and RANS are compared with experimental data. Wherever possible, comparison

from more than one calculation is shown. For more details on the computations or experiments, the original references cited may be seen.

7.4a *Transonic interactions*: Viscous effects on airfoils, even under attached flow conditions, can be significant at transonic speeds. An example of such effects on a supercritical airfoil is shown in figure 39; also included are comparisons from interactive calculations due to Stanewsky *et al* (1981). The calculations employ a potential flow modelling for the outer flow, an integral method due to Rotta (1968) for the boundary layer flow, and a triple-deck analysis (Inger & Mason 1976) to model shock-boundary-layer interactions. Results of calculations, with and without the triple deck analysis, are also included in figure 39. The observed double-shock system is fairly well-predicted when the local effects of shock-boundary-layer interaction are included in the calculation.

The two experimental flows in a transonic channel discussed in §§ 5.3 and 5.4 have recently been computed by La Balleur & Blaise (1985). Their calculations are based on an Euler solver for the outer inviscid flow and an integral type method for the viscous flow with an allowance for normal pressure gradients. Approximate transport equations for turbulent shear stress and turbulent kinetic energy are employed for modelling turbulence.

Results for surface pressure distributions for the case of weak separation at $M_l = 1{\cdot}3$ show (figure 40) reasonably good agreement (in figures 40 and 41, the streamwise distance is normalized by channel height, B). Detailed comparisons indicate (La Balleur & Blaise 1985) that both δ^* and H are somewhat overpredicted in the calculation. For the asymmetric channel flow at $M_l = 1{\cdot}37$ involving massive separation, comparisons are shown in figures 41 and 42. There is an overshoot of surface pressure near separation, and the pressure plateau is less well-defined; for $x/B \gtrsim 3$, δ^* prediction is considerably lower than the data. The nonequilibrium effects in this flow, mentioned briefly in § 5.4, are shown in figure 42. The transport

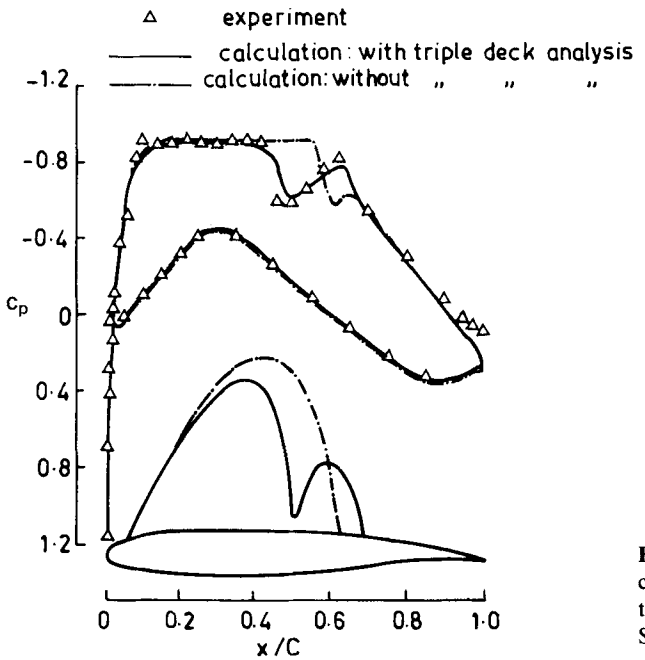

Figure 39. Experimental and computed surface pressure distributions: $M_\infty = 0.76$ (from Stanewsky *et al* 1981).

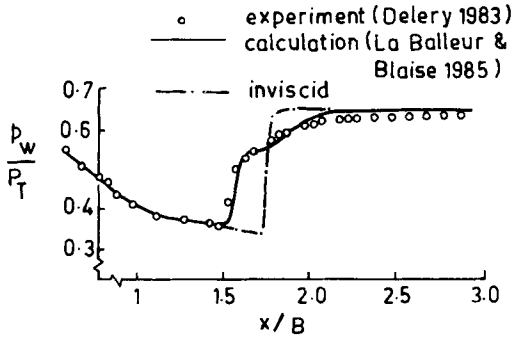

Figure 40. Experimental and computed surface pressure distributions: $M_l = 1.30$ (from La Balleur & Blaise 1985).

models used seem to reflect the experimentally observed behaviour in the separation region but are deficient in the reattachment and relaxation zones.

In the numerical calculations of flows involving strong normal shock waves, it is often very important to simulate precisely the downstream boundary condition. The back pressure in the subsonic flow can play a significant role in defining the gross features of the interactions. In the calculations presented in figures 40 to 42, the back pressure was so selected for each flow that the beginning of the compression at the foot of the shock wave matched the experimental data.

The turbulent separated flow on a flat plate (discussed in § 5.1) at $M_o = 1{\cdot}47$ have been computed using RANS (Viegas & Horstman 1978) employing zero-, one-, and two-equation models. All three models appear to predict the pressure rise upto

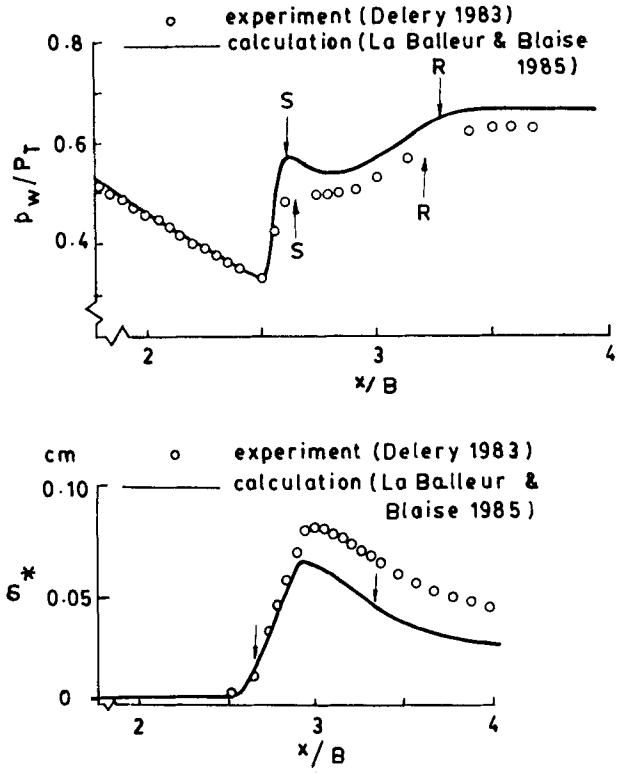

Figure 41. Experimental and computed surface pressure and displacement thickness distributions: $M_l = 1.37$ (from La Balleur & Blaise 1985).

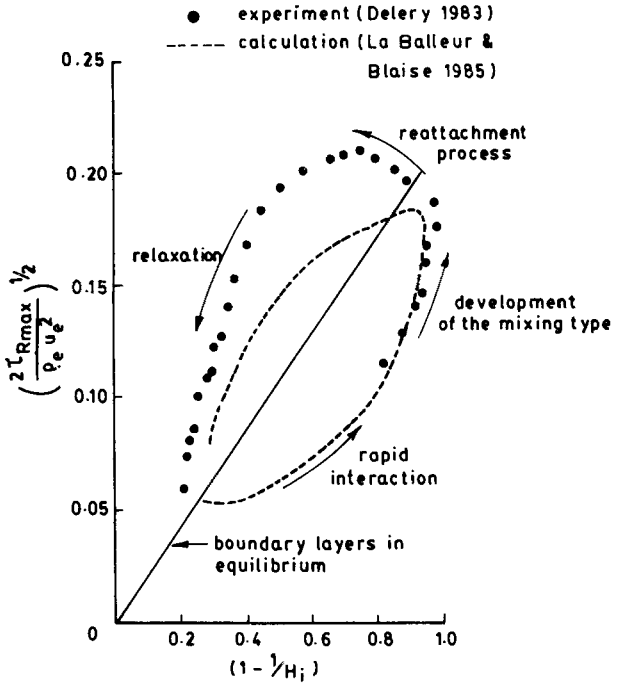

Figure 42. Evolution of maximum shear stress with equilibrium shape parameter for shock separated flow: $M_l = 1.37$ (from La Balleur & Blaise 1985).

separation reasonably well, but they all depart from the measurements downstream (figure 43). The velocity profile comparisons (Viegas & Horstman 1978) did not reveal any consistent picture amongst the three models; considerable disagreement was evident for different models in different regions of the flow. As in the previous case of massive separation, comparisons demonstrate again the inadequacy in modelling turbulence.

An example of a successful RANS calculation for a periodic separated flow at transonic speeds is shown in figures 44 and 45. Experiments on a thick circular arc airfoil in a high Reynolds number channel (with contoured top and bottom walls)

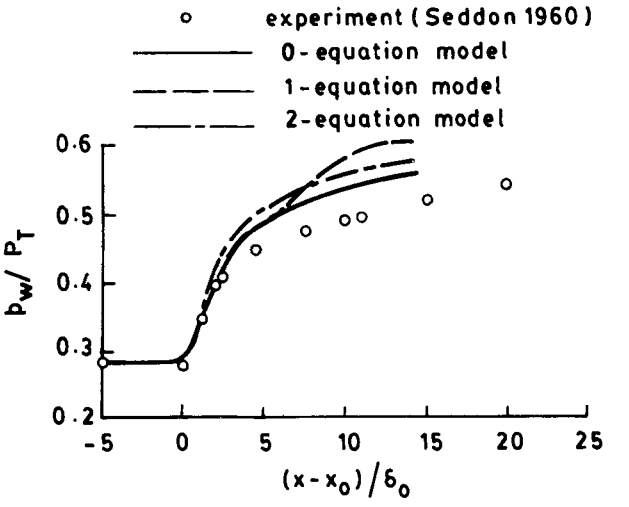

Figure 43. Comparison of experimental and computed surface pressure distributions: $M_o = 1.47$, $Re_{\delta_o} = 5.3 \times 10^4$ (from Viegas & Horstman 1978).

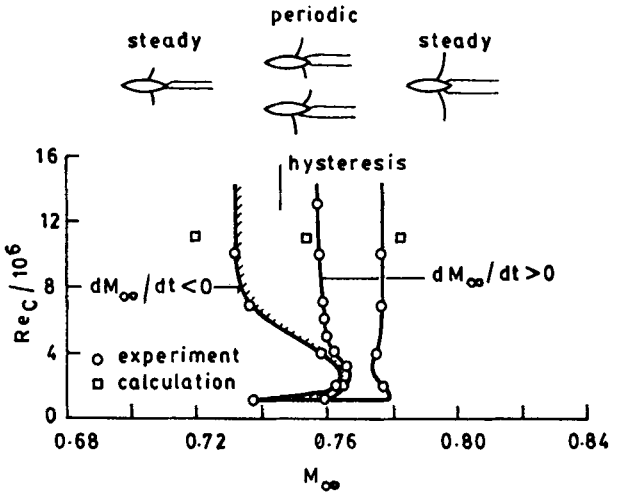

Figure 44. Experimental flow domains for a 18% thick circular arc airfoil (from McDevitt *et al* 1976).

revealed oscillatory flow, switching between shock-induced separation and trailing-edge flow separation in a narrow Mach number range (figure 44). On either side of the unsteady zone, the flow was relatively steady. Levy (1978) made calculations at three values of M_∞ of 0·720, 0·754 and 0·783 (figure 44), using an algebraic eddy viscosity model. These calculations revealed the observed steady flow at $M_\infty = 0{\cdot}72$ and 0·783 and periodic flow at $M_\infty = 0{\cdot}754$. Figure 45 shows comparisons of surface pressure variations with time at four locations on the airfoil for the unsteady case. Excellent reproduction of the unsteady pressure, including the phase difference between the upper and lower surfaces of the airfoil, may be seen in the calculations. The frequency of oscillations from predictions agreed within about 20% of the measured value.

The success of the calculation with a simple turbulence model described above may seem surprising since the evidence to-date suggests that none of the turbulence models available can satisfactorily predict flow with significant separation. A possible explanation is that, in the unsteady regime, the oscillations are sustained

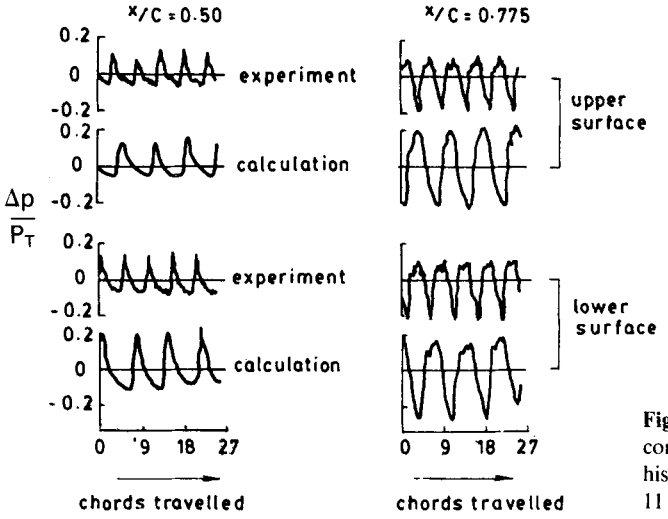

Figure 45. Experimental and computed surface pressure-time histories: $M_\infty = 0.754$, $Re_{c'} = 11 \times 10^6$ (from Levy 1978).

by the outer flow (inviscid mechanisms), and the turbulence modelling is only important to the extent that the separation which is necessary for triggering the large scale unsteadiness is induced in the calculation.

Recently Purohit (1987a) has computed levels of surface pressure fluctuations (at $M_\infty = 0.8$) arising from shock oscillations on a bulbous payload shroud using RANS and an algebraic turbulence model. Although the paper does not contain comparison of calculated unsteady properties with experiments, the computations have revealed interesting unsteady flow features on such a configuration.

7.4b *Supersonic interactions*: Turbulent separated flows induced by compression corners or ramps have been investigated by several authors at supersonic speeds. Experimental results for two ramp angles of 20 and 24° at $M_o = 2{\cdot}8$ are compared with calculations in figures 46 and 47. RANS computations, employing a version of McCormack's algorithm, have been made (Viegas & Horstman 1978) for both cases, while the 24° case has been computed recently using the interactive method of La Balleur & Blaise (1985) discussed previously. The turbulence models used with the RANS are indicated in the figures.

For the 20° ramp, pressure distributions are reasonably well-predicted by the two-equation models, while the skin friction predictions seem deficient downstream of reattachment. For the flow with large separation (24° case), again, the predictions with two-equation models are relatively better than the zero- and one-equation models, but are still deficient in an overall sense. The results from the interactive method are comparable to those obtained using the two-equation

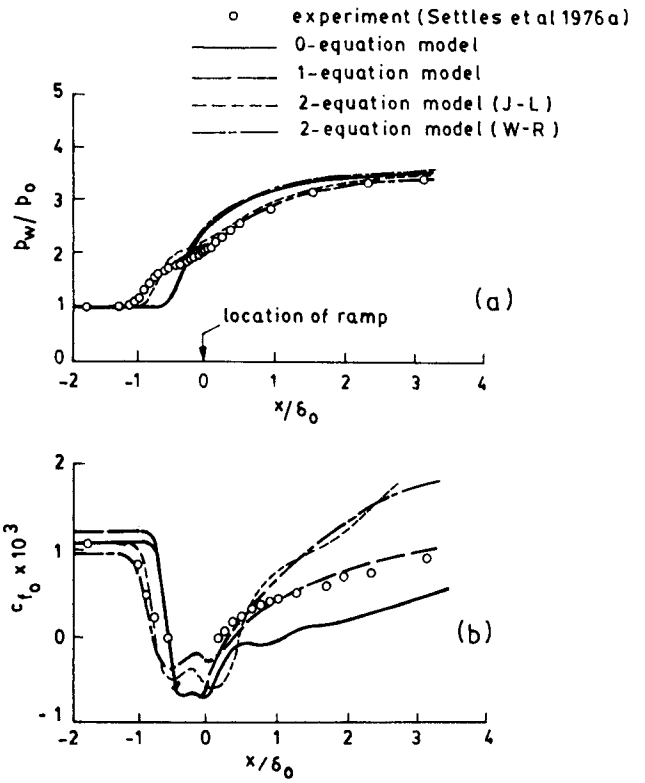

Figure 46. Comparison of experimental and computed surface data: $M_o = 2.8$, $Re_{\delta_o} = 1.65 \times 10^6$, $\alpha = 20°$ (from Viegas & Horstman 1978), (**a**) surface pressure, (**b**) skin friction.

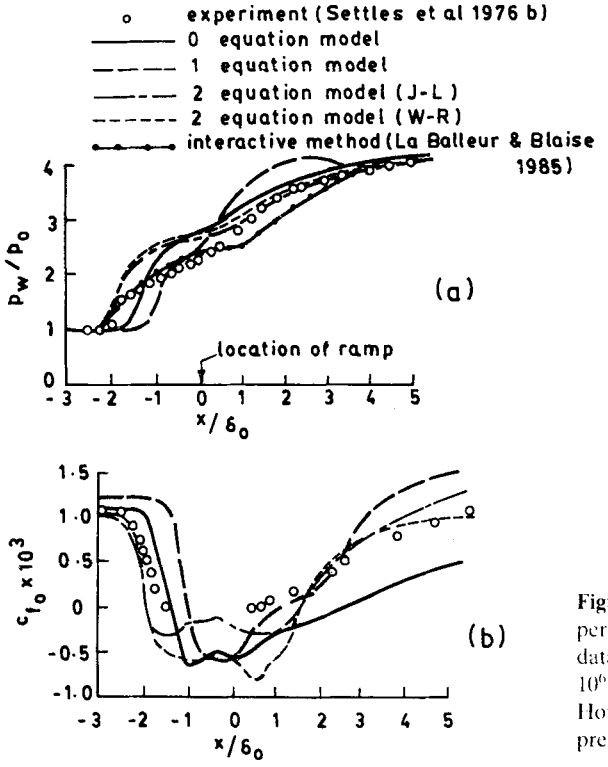

Figure 47. Comparison of experimental and computed surface data: $M_o = 2.8$, $Re_{\delta_o} = 1.33 \times 10^6$, $\alpha = 24°$ (from Viegas & Horstman 1978). (a) surface pressure, (b) skin friction.

models. Surface pressure fluctuation measurements made recently (Dolling & Or 1983) for the two flows have revealed a certain unsteady character of these flows; to what degree this might influence the mean flow field is still an important question to be answered.

The importance of accounting for the history effects of turbulence in flows undergoing rapid pressure gradients hardly needs to be stressed. Attempts have also been made to modify, for example, the zero-equation eddy viscosity model to reflect history effects in an approximate sense. Figure 48 shows comparisons of measured surface pressure distributions with RANS calculations (Shang & Hankey 1975) for a 25° ramp at $M_o = 2{\cdot}96$. Predictions have been made with three versions of the zero-equation model; (i) the Cebeci-Smith equilibrium model, (ii) a frozen model, and (iii) a relaxation model. The frozen model concept is relevant in flows undergoing rapid pressure gradients (e.g. Narasimha & Srinivasan 1973). In the relaxation model, the Reynolds stress relaxation phenomena are described by a simple algebraic equation for the eddy viscosity coefficient, which involves a relaxation length scale λ to be described empirically; a value of $\lambda = 10\ \delta_o$ based on available information has been chosen in these calculations (Shang & Hankey 1975).

The equilibrium and frozen models predict small and large separated regions, respectively. The relaxation model, on the other hand, shows significant improvement in a relative sense; the need for further refinements is also clear. Similar success with an algebraic relaxation model is also seen in the calculations of separated flows caused by impinging shock waves (Shang *et al* 1976).

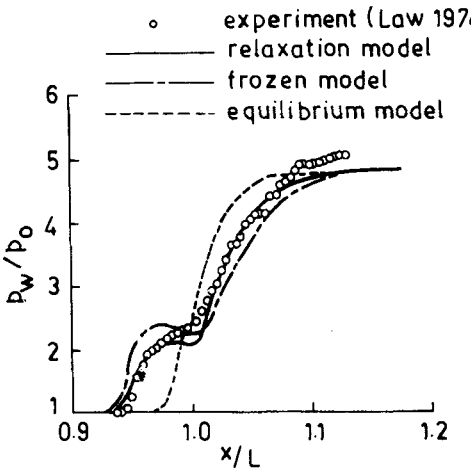

Figure 48. Comparison of experimental and computed surface pressure distribution: $M_\infty = 2.96$, $Re_L = 10^7$, $\alpha = 25°$ (from Shang & Hankey 1975).

The current state-of-the-art in computing two-dimensional shock-boundary layer interactions may be summarized as follows. As long as the separated region is small $[0(\delta_o)]$, both interactive and RANS seem to perform equally well in an engineering sense. The wall pressure distributions can be predicted by any model, while the two-equation models give better predictions of the skin friction distributions. For flows involving large scale separation, significant improvements in modelling the dynamics of turbulence are necessary, and in general, calculations based on RANS equations may be preferable; significant pressure variations normal to the flow which arise in these flows are well-handled by RANS.

Although certain broad conclusions are drawn above based on the examples discussed, some caution is required in the assessment of the calculation methods in general. To perform a clean experiment with massive separation is not an easy task. As discussed in § 4.5, unless sufficient care is taken, some degree of three-dimensionality is present even in nominally two-dimensional flows; an assessment of the departure from two-dimensionality is essential before conclusions about the prediction method can be drawn. The experimentally observed large-scale unsteadiness in the separated flows involving shock waves, which is not accounted for in the methods of calculation, could lead to differences between calculation and experiments.

8. Control of shock-wave-boundary-layer interaction

Separation control by active or passive means is often desirable and some times necessary for improving aerodynamic performance. The use of suction and tangential blowing for separated-flow-control is known for several decades. Suction removes low momentum fluid in the boundary layer near the wall thereby providing sufficient energy in the fluid close to the surface to overcome adverse pressure gradients. Tangential blowing through a narrow slot, as commonly used, energizes the boundary layer near the wall providing sufficient kinetic energy to negotiate adverse pressure gradients. It may be useful to incorporate suction and tangential blowing in a single device (or system) to exploit the benefit from both schemes.

In the context of shock-boundary-layer interaction control, there have been several studies dealing with suction and tangential blowing in the different speed regimes; a brief account of some of these may be found in the book by Chang (1976). Most of the investigations even to-date have been either exploratory in nature or focussed towards some design application. Systematic studies of these control techniques with regard to "basic interactions" are rather few. Many questions remain both from the point of view of general understanding and of applications.

In this section, a brief overview of the developments in control techniques using suction and blowing is presented. A more detailed review of the subject may be found in the recent article by Delery (1985).

8.1 *Applications of tangential blowing*

Tangential blowing for control of shock-boundary layer interaction has been studied by several investigators (e.g. Chinneck *et al* 1955; Peake 1966; Wong & Hall 1975; Wong 1977; Viswanath *et al* 1977, 1983; Schwendemann & Sanders 1982). These studies have revealed that blowing is generally effective in controlling shock-induced separation in both two-dimensional and axisymmetric flows. Since very few systematic studies on simpler geometries exist in the literature, our understanding of some of the general features of the flow field and of the parameters that may influence the effectiveness of blowing are still somewhat unclear.

8.1a *Parameters governing blowing performance*: Since blowing involves injection of additional mass and momentum into the boundary layer, the parameters affecting its performance include the jet velocity, its density and the slot width b in two-dimensional flows (figure 49). The most widely used parameter is the blowing momentum coefficient, C_μ defined by

$$C_\mu = \dot{m}_j u_j / \rho_o u_o^2 \theta_o,$$

where $\dot{m}_j$ is the jet mass flow rate, u_j is the jet velocity, ρ_o is the free stream density, u_o is the free stream velocity and θ_o is the boundary layer momentum thickness ahead of the interaction. Some investigators in the past have also used an excess blowing momentum coefficient, defined in figure 49.

Figure 50 shows an example (Wong & Hall 1975) of the effectiveness of a tangential blowing system consisting of discrete jets in controlling separation in a supersonic inlet at $M_\infty = 2{\cdot}0$. A significant reduction in the separated region may be inferred from the surface pressure distributions even for a value of $C'_\mu = 0{\cdot}9$; their results also showed an appreciable improvement in the total pressure recovery and a low flow distortion for $C'_\mu = 1{\cdot}5$.

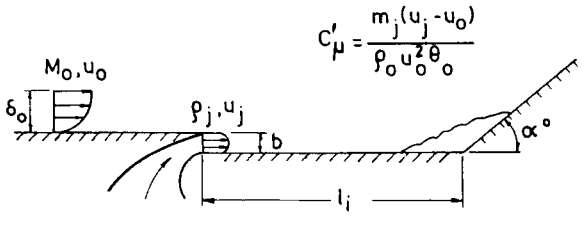

Figure 49. Sketch defining notation used with tangential blowing.

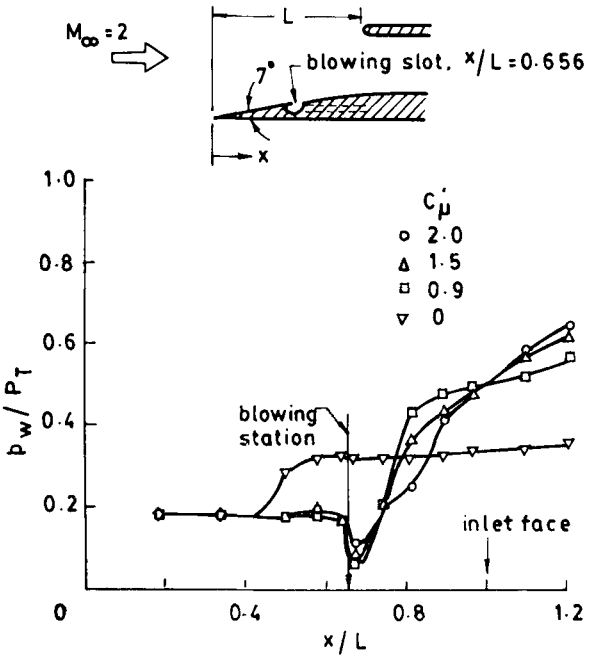

Figure 50. Ramp centreline pressure distributions: $M_\infty = 2.0$ (from Wong & Hall 1975).

There have been some attempts (Grin 1967; Lakshmikantha *et al* 1969) to suggest correlations for blowing effectiveness based on their own limited data. It is interesting to touch upon the correlation presented by Lakshmikantha *et al* (1969). Based on a series of experiments involving impinging shock waves at $M_\infty = 2{\cdot}2$ and 2·6, they presented a correlation for the minimum blowing pressure ($\hat{P}_i$) required to suppress separation which is of the form (figure 51),

$$\hat{P}_i = 1{\cdot}25\,\Delta p\ (l_i/\delta_0)^{0.70},$$

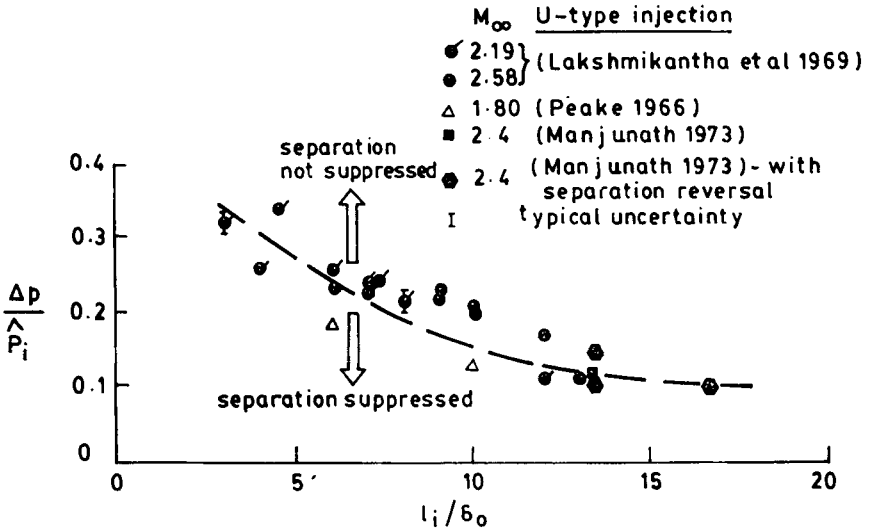

Figure 51. Correlation of minimum injection pressure required to suppress separation (from Lakshmikantha *et al* 1969).

where Δp is the observed pressure rise across the shock wave, l_i is the distance between the injection slot and shock intersection point on the wall in inviscid flow and δ_o is the boundary layer thickness ahead of interaction. It is interesting to note that, unlike the mass or momentum coefficient, the above correlation does not involve the slot width b; in these tests, b/δ_o was varied betwen 0·1 and 0·4. Although the data shown in figure 51 are suspected to have some interference effects (Viswanath *et al* 1977, 1983), the trend indicates that the total mass or momentum injected may not be an important factor at least for improving the surface pressures in the separated flow; it is likely that the excess velocity injected is the dominant factor.

8.1b *Location of blowing slot*: Among the various factors that may determine the effectiveness of injection, several studies (Peake 1966; Krishnamurthy 1973; Manjunath 1973), have revealed that the injection slot location is a critical parameter. We shall examine this aspect in some detail.

At the outset it is convenient to distinguish between two types of injection depending on the location of the injection slot (figure 52):

1. *U*-type: injection is upstream of where the separation point would have been in the absence of injection (i.e., the conventional location adopted for boundary-layer control).
2. *D*-type: injection is downstream of the same point, but within the recirculating (or "dead air") zone.

Based on detailed experiments at a free stream Mach number of 1·8 with *U*-type injection, Peake (1966) made an important distinction between wall flow reversal and wake (or outer flow) reversal, and found that there was an optimum slot location at which both wall and wake flow reversals were avoided. For his experimental conditions, this optimum was at $l_i \simeq 6\delta_o$.

The experiments of Krishnamurthy (1973) and Manjunath (1973) with *U*-type supersonic injection to control separation at a compression corner revealed some interesting and unexpected features. The first is what may be called "separation reversal"; with increase in injection total pressure P_i, the extent of separation first decreases and then increases (as inferred from wall static pressure distributions) after a certain value of P_i, which seems to depend on l_i and on the compression corner angle (all other conditions remaining the same). This puts a serious limitation on the range of P_i that can be usefully employed to suppress separation. The second feature is that the upstream influence or the extent of separation in the absence of injection was much larger than would be expected from earlier observations with similar flow conditions and ramp angles. It was demonstrated (Sagdeo 1974) that this abnormal upstream influence was due to the effects of the injection slot geometry on the oncoming boundary layer, which acts as a backward-facing step in the absence of injection.

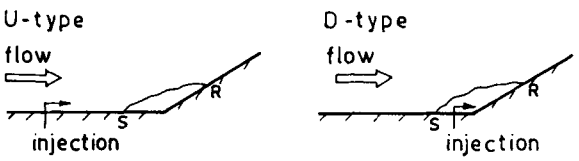

Figure 52. Sketch showing *U*- and *D*-type tangential injection.

8.1c. *Experiments with D-type blowing*: Although there was some indirect evidence (Chinneck *et al* 1955; Wong 1977) that *D*-type injection could be useful, a quantitative assessment of its effectiveness resulted from the investigations of Viswanath *et al* (1977, 1983). They studied *D*-type injection (by design) for two values of l_i namely, 0·77 δ_o and 1·54 δ_o at a ramp induced turbulent separated flow at $M_o = 2{\cdot}5$.

Figure 53 shows surface pressure distributions with and without injection for $l_i = 1{\cdot}54\,\delta_o$. A monotonic increase in the maximum slope of the pressure distributions with increasing P_i is evident and suggests a progressive reduction of the length of the separation bubble. Similar results were seen at $l_i = 0{\cdot}77\,\delta_o$. Measured Mach number profiles in the interaction region for the case $l_i = 1{\cdot}54\,\delta_o$ (figure 54) shows conclusively the absence of wake flow reversal as well, suggesting complete suppression of boundary layer separation.

Effectiveness of *D*-type injection for the above experiments was assessed using two measures; (i) a suitably defined "reattachment length", Δ_r (figure 55), which is related to the bubble size Δ_b (Manjunath 1973) and (ii) the pressure recovery coefficient c_{p_r} defined as

$$c_{p_r} = (p_{\mathrm{ref}(i)} - p_{\mathrm{ref}(o)})/(p_d - p_{\mathrm{ref}(o)}),$$

where $p_{\mathrm{ref}(i)}$ and $p_{\mathrm{ref}(o)}$ denote the static pressures at a reference location on the ramp with and without injection, respectively.

Figures 55 and 56 show the variation of normalized reattachment length and the pressure recovery coefficient with injection pressure ratio (for both values of l_i) with *D*-type injection. These results are compared with those of Krishnamurthy (1973) and Manjunath (1973) who used *U*-type injection under essentially the same conditions as those in the experiments of Viswanath *et al* (1977, 1983). These

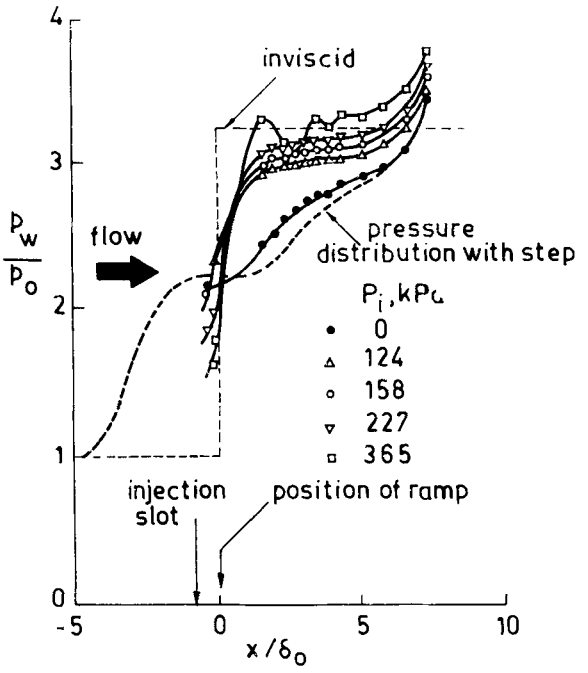

Figure 53. Wall static pressure distributions with injection: $M_o = 2.5$, $l_i = 1.54\,\delta_o$ (from Viswanath *et al* 1983).

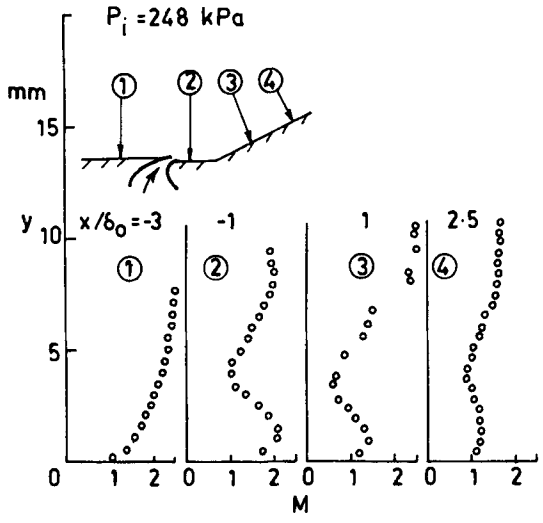

Figure 54. Mach number profiles in the interaction region with injection: $M_0 = 2.5$, $l_i = 1.54\delta_0$ (from Viswanath *et al* 1983).

comparisons show clearly the superiority of *D*-type over the *U*-type injection. In these experiments, the mass and momentum flux in the jet needed to suppress separation is estimated to be only about 18 and 14% of that in the oncoming boundary layer.

The success of the *D*- over the *U*-type injection suggests that mechanisms, other than energizing the boundary layer near the wall upstream of the beginning of adverse pressure gradients (as in the conventional *U*-type), exist for effective separation control. It has been speculated (Viswanath *et al* 1983) that an important factor in the *D*-type injection is the interaction of the jet injected at high total

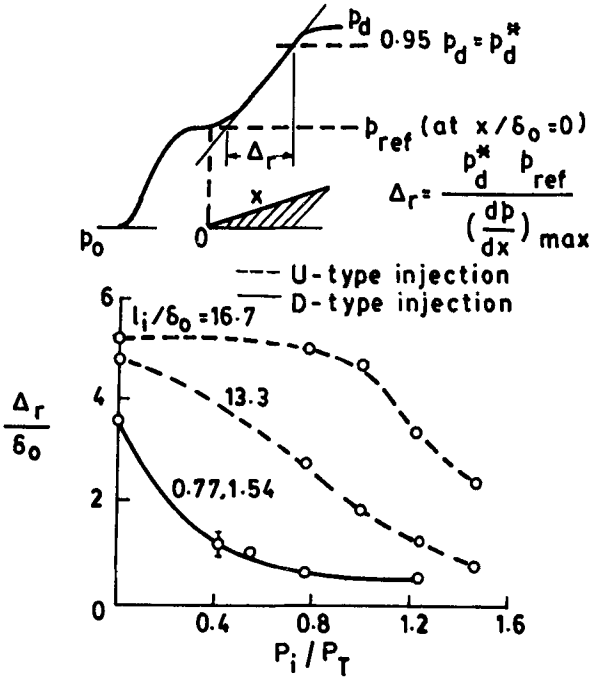

Figure 55. Variation of reattachment length with injection (from Viswanath *et al* 1983).

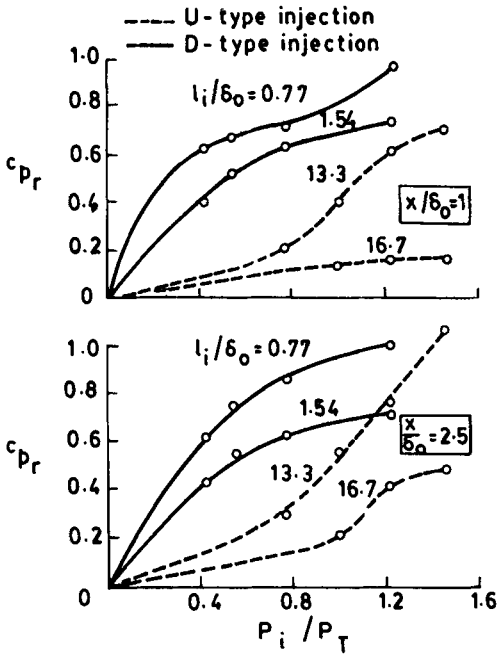

Figure 56. Static pressure recovery in the reattachment region with injection (from Viswanath *et al* 1983).

pressures with the (otherwise reverse flow) boundary layer, leading to eventual removal of the reattachment point. It is likely that the entrainment of the recirculating flow by the jet may play a role in the mechanisms involved.

8.1d *Calculation methods*: The problem discussed here certainly presents complexity in flow modelling and in calculation methods. There has been hardly any attempt to calculate these interacting turbulent flows with tangential fluid injection at high speeds. From an engineering viewpoint, a viscous-inviscid interactive type of calculation, with the viscous flow represented by an integral method, may be adequate. Even with *U*-type injection, there is insufficient mean flow data at high speeds covering a range of flow and geometrical parameters to enable construction of a reliable integral method. Experience gained in calculating low speed wall jet flow fields in adverse pressure gradients (Gartshore & Newman 1969; Hubbart & Bangert 1970; Yegna Narayan & Narasimha 1973) could be utilized as a first step in predicting these viscous flows at high speeds. With *D*-type injection, the complexity may be even greater, and further understanding of the physical mechanisms at play is essential before any modelling or calculation method can be formulated.

8.2 *Application of suction*

Boundary layer suction is a powerful tool (useful in many different speed regimes) for controlling flow separation, apart from the other engineering applications it has. Fluid near the wall is removed through slots or perforations, so that the new boundary layer which is formed downstream of the suction zone can withstand the imposed adverse pressure gradients. Suction generally leads to a fuller velocity profile and a consequent reduction of the boundary layer thickness. As with blowing, suction involves energy investment, and it is important in applications to

determine the "minimum suction volume" or the power required to drive the suction pump.

Several exploratory studies dealing with suction for control of shock-boundary layer interactions have been reported (e.g. Pate 1969; Seebaugh & Childs 1970; Tanner & Gai 1970; Mathews 1970; Wong 1974; Fukuda *et al* 1977). These studies, while showing the general effectiveness of suction in the various situations studied, contain little information on flow-field behaviour. Even engineering correlations for suction effectiveness do not seem to have been attempted; this situation is perhaps undesirable, since suction adds several new geometrical parameters to the problem, which even otherwise is complex enough. In this section, we shall present examples of application of suction and bleed (the distinction between the two being that bleed does not require energy input but could still drain energy) for the control of shock-boundary-layer interactions, and include an assessment of the state of the calculation methods.

8.2a *Parameters governing suction-performance*: It is common practice to define a suction quantity coefficient given by

$$C_Q = Q/Au_o,$$

where Q is the total volume rate of fluid removed, A denotes the wetted area and u_o is the free stream velocity. For the case of uniform suction (with a suction velocity of $-v_w$).

$$C_Q = -v_w/u_o$$

As with tangential blowing, for a given shock pressure rise and upstream flow conditions, the suction performance would, in general, depend on where the fluid is sucked in relation to the interaction zone, the total mass flow removed and the suction arrangement. At least three different arrangements have been employed in the various investigations; they include porous (or perforated) wall suction, slot suction and scoop suction. Several geometrical parameters are associated with each of the above suction configurations. For example, perforated wall arrangement (which is widely used) is defined by the number of bleed holes, their shape, diameter and distribution; with slot suction, the width and number of slots, and their orientation and distribution, are relevant parameters. For each of the configurations, the plenum or bleed chamber geometry could have an added influence. In view of the fairly large number of parameters associated with a suction device, perhaps it may not be worthwhile to attempt generalized engineering correlations for effectiveness even in the context of basic interactions.

8.2b *Location of suction system*: As may be expected, the location of suction in relation to the interaction zone is an important factor governing suction effectiveness. Since suction is often applied over a finite distance (in the range of several δ_o), the definitions U- and D-type (described in § 8.1b) may not be strictly applicable; we shall therefore use a much broader concept for suction location in the examples to follow.

Mathews (1970) investigated the effects of suction in an (internal) axisymmetric conical shock-wave-boundary-layer interaction at $M_\infty = 2{\cdot}0$. The suction geometry consisted of one row of perforated holes located around the circumference and

suction was applied "within" the interaction region. Both the shock strength and the mass flow sucked were varied in his experiments. Figure 57 shows a schematic of the wave pattern, measured wall static pressures and c_f distributions in the interaction region, both with and without suction, for a separated flow generated by a 30° (total apex angle) cone. With a bleed mass flow of 7·5% of the approaching boundary layer mass flow, separation was nearly suppressed; the skin friction distributions show much higher values as a result of suction.

In a similar test set-up (Seebaugh & Childs 1970) at $M_\infty = 3{\cdot}8$, a separated zone (of length approximately $2\,\delta_o$) could be controlled with a bleed mass flow rate of 3% of the boundary layer mass flow rate with suction applied "within" the interaction zone (figure 58). In this experiment, the suction geometry was similar to that used by Mathews (1970), but had four rows of perforated holes around the circumference and distributed over a length of about $1{\cdot}5\,\delta_o$. It was also found that a similar suction performed "upstream" of the interaction region was less effective.

Detailed experiments to determine the effects of bleed geometry and bleed rate on the boundary layer development following shock-boundary-layer interaction in an axisymmetric mixed compression inlet at $M_\infty = 2{\cdot}5$ revealed (Fukuda *et al* 1977) that suction performed "upstream or downstream" of the interaction zone was more beneficial than "within"; this assessment was made by examining the shape factor following the interaction. This observation, which is in contrast with those of Mathews (1970) and of Seebaugh & Childs (1970), might be a result of several differences in the bleed geometries used in the three experiments. Furthermore, the flow studied by Fukuda *et al* (1977) was more complex, involving multiple shock reflections between the centre body and the inlet cowl.

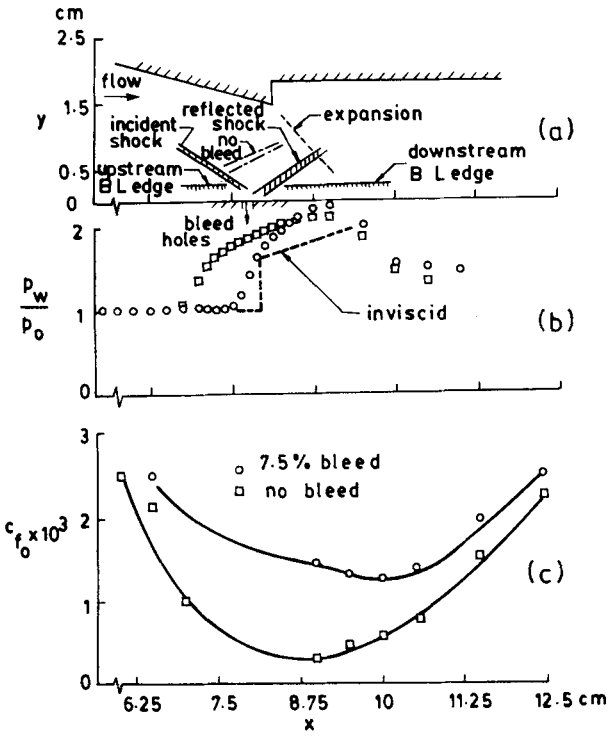

Figure 57. Effect of suction in an axisymmetric shock-boundary layer interaction: $M_\infty = 2.0$ (from Mathews 1970), (**a**) wave pattern, (**b**) wall pressure distribution, (**c**) skin friction distribution.

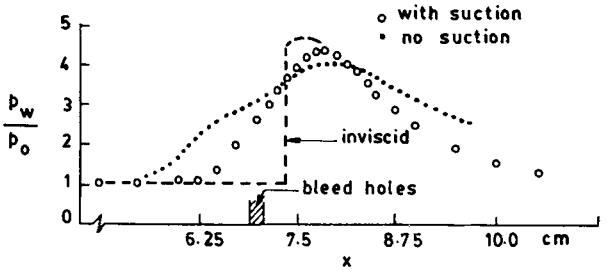

Figure 58. Effect of suction on wall static pressure distribution: $M_\infty = 3.78$ (from Seebaugh & Childs 1970).

The experiments of Wong (1974) in an axisymmetric external compression inlet at $M_\infty = 2{\cdot}0$ also showed the effectiveness of suction performed both "upstream" and "within" the interaction region; suction was applied in a (nearly) continuous fashion in these tests.

The results discussed above suggest that suction "within" the interaction zone can be quite effective; there is very little information in the literature at comparable conditions to make a better judgement on the best location for suction. The bleed system arrangement can be expected to influence the overall performance associated with suction.

Effects of slot suction, with the slot located "within" a separated flow, have been studied by Tanner & Gai (1970) at $M_o = 1{\cdot}93$. The suction slot, formed between the flat plate and the ramp under surface, was varied in the tests; there was also provision for varying suction mass flow independently. An example of the effectiveness of *D*-type suction for a 16° ramp is shown in figure 59 for different values of suction coefficient (defined in figure 59). Progressive increase in the surface pressure recovery and reduction in the upstream influence with increasing suction rate is evident. For a value of suction coefficient of 1·5 (for which the inviscid pressure level is reached), the mass flow removed corresponds to about 20% of the mass flow in the approaching boundary layer. Qualitatively similar effects of suction were seen at other ramp angles.

8.2c *Examples of natural bleed*: Natural bleed has many similarities with suction and does not involve any power input. The high pressure in the (separated) dead air zone, if vented to a low pressure region, causes natural bleed or suction of the mass flow from the dead air region, leading to an effective suppression of the separated flow. This is a case of *D*-type suction or bleed in the sense defined in § 8.1b. Several studies employing *D*-type bleed have been conducted (e.g. Crawford 1961; Ball & Korkegi 1968; Ball 1970). Results from Ball & Korkegi (1968) and Ball (1970) are shown to illustrate the suction effectiveness in such cases.

Ball & Korkegi (1968) studied effects of suction through a 2D slot at a compression corner, formed by a flat-plate-flap combination (figure 60) at a hypersonic Mach number of 12·3 and with laminar boundary layer conditions. The slot formed at the intersection of the flat plate and flap could be varied in width providing a variation of bleed mass flow. The effects of suction for various ramp angles were examined. Static pressure distributions for a 20° flap deflection angle (shown in figure 60) indicate a progressive decrease in the extent of the separated region with increasing values of slot width d^* (or bleed mass flow); the pressure distribution corresponding to $d^* = 0{\cdot}22$ cm resembles the inviscid case. In a later

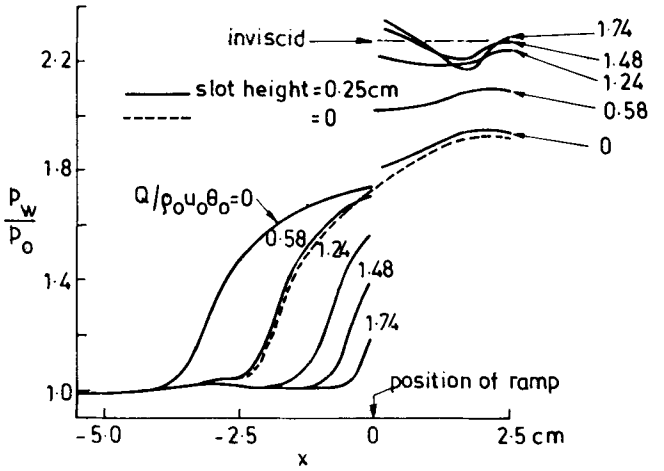

Figure 59. Wall static pressure distributions with slot suction: M_o = 1.93, α = 16° (from Tanner & Gai 1970).

study, Ball (1970) showed the effectiveness of the *D*-type bleed (discussed above) at other values of M_o in the range 5 to 8. A simple correlation (figure 60) for the minimum mass flow to be removed for complete suppression of separation was given by Delery (1985).

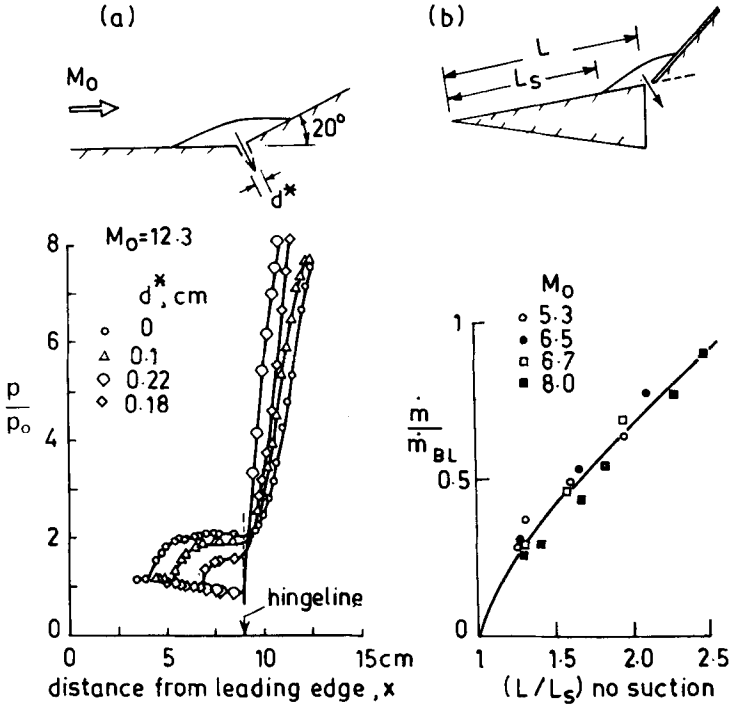

Figure 60. Effect of natural bleed on ramp-induced shock boundary layer interaction: (**a**) surface pressure distributions (from Ball & Korkegi 1968), (**b**) correlation of suction mass flow for suppression of separation (from Delery 1985).

8.2d *Calculation methods*: Methods for the calculation of boundary layer development with distributed or porous suction are fairly well-developed (Schlichting 1968). Porous suction, which can be realized in practice without much difficulty, offers the simplest boundary condition at the wall; it is common practice to prescribe the transpiration velocity ($-v_w$) as a function of the streamwise distance. In experiments, the suction velocity is often estimated from certain gross measurements (mass flow, pressure etc) in the bleed chamber. For other suction arrangements involving either slots or perforations, the flow through these devices is sufficiently complex such that an estimation of appropriate suction velocities at the wall becomes very difficult. There are very few experimental investigations wherein attempts have been made to get some idea of the flow development through the devices. So, the central problem in the calculation of effects of mass transfer at the wall is concerned with the estimation of the true boundary condition appropriate to the device.

For turbulent-shock-boundary-layer interactions with suction, there has been no attempt to calculate the flow using RANS to the author's knowledge. Effects of porous suction on laminar shock-induced separated flows have been studied using RANS by Tassa & Sankar (1979) and Purohit (1987b). The calculations made by Purohit (1987b) show that vectored porous suction can be more beneficial than normal suction. Don Gray & Maus (1981) have extended the Lees & Reeves (1964) interaction method to the calculation of slot suction at a ramp-induced laminar separated flow at $M_\infty = 6{\cdot}7$. Their calculations, assuming uniform flow through the slot, indicate moderate agreement with the data of Ball (1970).

Engineering methods to calculate the variations of certain gross parameters of the flow through the interaction have been attempted. Seebaugh *et al* (1968), using a control volume approach and an integral method of analysis, present results for the changes in boundary layer thickness, velocity profile shape and other thickness parameters across the interaction; they consider porous, single slot as well as scoop suction configurations. Their paper, however, contains very limited comparisons with experiments, perhaps because of paucity of reliable data. The approach is further extended by Sun & Childs (1974) to treat successive shock reflections between an axisymmetric centre body and an outer circular cowl, including small amounts of suction at the location of the second shock-boundary layer interaction zone. Their results show fair agreement with experimental data for small bleed rates of about 3% of the boundary layer mass flow.

To summarize, considerable difficulty exists in dealing with the problem of the shock-turbulent boundary layer interaction with mass transfer at the wall. The problems include formulation of the wall boundary condition for different suction configurations, and modelling turbulence as affected by the mass transfer at the wall.

9. Concluding remarks

Although considerable amount of research has been carried out on the problem of shock-wave-boundary-layer interaction, our general understanding of turbulent interactions and Reynolds number effects in particular still remains poor. The progress is hampered primarily by our inadequate knowledge of turbulence dynamics in these complex flows. In the author's opinion, the principle of "free

interaction" (now known for over three decades) still remains a significant step in the understanding of high speed separated flows, despite the progress that has been made on the various fronts. There is now growing evidence that fully separated turbulent flows in reality are inherently unsteady and 3D to some degree; the idealization that the mean flow is 2D and steady may be an over-simplification.

Use of modern diagnostic techniques like laser velocimetry has provided valuable information on the complex behaviour of turbulence in these interactions. Similarly, sophisticated computer codes are now available for predicting these flows including regions of small separation which are of value to an engineer. Regarding turbulence modelling, accounting rationally for history or nonequilibrium effects and shock effects on turbulence appear to be important to achieve any success in computing separated flows; systematic research at high speeds of the kind reported by Narasimha & Prabhu (1972) investigating memory effects of large scale structures should prove valuable. Both surface and flow-field measurements investigating the unsteady character of shock-separated flows are necessary before modelling of large scale unsteadiness associated with shock waves can even be attempted.

Shear layer reattachment, being a key element in the dynamics of separated flows, has received very little attention in the literature. The role played by viscosity in the reattachment process is still an open question. It would be informative to examine if the general ideas of free interactions can be extended to the reattachment process; in particular, to see if the pressure rise to reattachment and the pressure distribution in the reattachment region can be related to the properties of the shear layer approaching reattachment for different shock-separated flows at supersonic/hypersonic Mach numbers.

On control techniques employing tangential blowing and suction, the available evidence suggests that interference with the flow in the separated zone or bubble can lead to effective separation control. With *D*-type injection, further research, both from the point of view of understanding the phenomena and assessing its effectiveness in other separating flows, is needed. Several interesting issues with regard to tangential blowing, including a suggestion for "intermittent blowing or blowing in puffs" have been discussed by Narasimha (1978). As regards suction "within" the interaction zone (or *D*-type suction), the mass imbalance created in the separated zone as a result of suction is likely to be a prime factor causing suppression of separation. Base-bleed causing base-drag reduction is a clear example of such a mechanism.

On the applications front, the situation is rather unclear regarding the best mode (or technique) for separation control. Such an assessment or judgement will have to be made on a case to case basis, giving due consideration to the energy input. For example, in applications where shock excursions are large, perforated wall suction spread over the required length is probably a good choice; on the other hand, if the location of the separated zone is in some sense stationary, *D*-type injection is an obvious choice. It would be rewarding to examine the usefulness of passive control techniques of the kind being investigated on transonic airfoils (e.g. Bahi *et al* 1983; Krogmann *et al* 1984) for shock-wave-boundary-layer interaction control in general.

Three-dimensional shock-boundary layer interactions are of greater interest in practical applications. Attempts to understand certain basic features of relatively simpler 3D interactions have begun in recent years (e.g. Oskam *et al* 1975; Settles *et*

al 1980; Dolling 1982). Since, in general, 3D separated flows are vortex-dominated, there is hope that turbulence modelling may not be as critical as in 2D flows, at least for certain 3D interactions (Horstmann & Hung 1979; Hung & Kordulla 1983). There is a definite need for systematic and focussed research in the area of 3D shock-wave-turbulent-boundary-layer interaction.

List of symbols

a_T stagnation speed of sound;
b slot width;
C airfoil chord;
c_f, c_p skin friction and pressure coefficients, respectively;
e mean voltage;
H boundary layer shape factor;
H_i incompressible shape factor;
k turbulent kinetic energy;
L model length;
l_o upstream influence interaction length (defined in figure 13);
l_b separation bubble length;
l^* interaction length (defined in figure 28);
l_i injection distance (defined in figure 49);
$\dot{m}$ mass flow rate;
M Mach number;
p static pressure;
P_i injection total pressure;
P_T tunnel stagnation pressure;
q dynamic pressure;
Re unit Reynolds number;
R reattachment point;
S separation point;
T temperature;
U, V instantaneous velocity components;
u, v mean velocity components;
u', v' fluctuating velocity components;
x, y coordinates along and normal to the wall;
α ramp or compression corner angle;
γ_p velocity intermittency;
δ boundary layer thickness;
δ^* boundary layer displacement thickness;
θ boundary layer momentum thickness;
ρ density;
τ_R turbulent shear stress;
τ_w wall shear stress;

Subscripts

BL oncoming boundary layer;
d conditions downstream of the interaction;

e conditions at the edge of the boundary layer;
i conditions of injected fluid;
is conditions at incipient separation;
l local conditions;
o conditions at the edge of the flat plate boundary layer just ahead of the interaction;
p conditions at the beginning of plateau region;
r conditions at reattachment;
s conditions at separation;
w conditions at the wall;
aw adiabatic wall;
∞ conditions at upstream infinity.

References

Ackeret J, Feldman F, Rott N 1946 Investigations of compressior. shocks and boundary layers in gases moving at high speed, NACA TM 1113

Adamson T C, Feo A 1975 *SIAM J. Appl. Math.* 29: 121–145

Adamson T C, Messiter A F 1980 *Annu. Rev. Fluid Mech.* 12: 103–138

Anyiwo J C, Bushnell D M 1982 *AIAA J.* 20: 893–899

Bachalo W D, Johnson D A 1979 An investigation of transonic turbulent boundary layer separation generated on an axisymmetric flow model, AIAA Paper 79-1479

Bahi L, Ross J M, Nagamatsu H T 1983 Passive shock-wave/boundary layer interaction control for transonic airfoil drag reduction, AIAA Paper 83-037

Ball K O W 1970 *AIAA J.* 8: 374–375

Ball K O W, Korkegi R H 1968 *AIAA J.* 6: 239–243

Beam R M, Warming R F 1978 *AIAA J.* 16: 393–402

Bradshaw P, Ferris D H, Atwell N P 1967 *J. Fluid Mech.* 28: 593–616

Brusseleers M 1980 *Shock-boundary layer interactions in turbomachines*; Von Karman Inst. (Belgium), Lecture Series 1980-8

Burggraf O R 1975 Flow separation, AGARD-CP-168, Paper no 10

Burggraf O R, Rizetta D, Werle M J, Vatsa V N 1979 *AIAA J.* 17: 336–343

Carter J E 1975 Inverse solutions for laminar boundary layer flows with separation and reattachment, NASA TR-R-447

Cebeci T, Meier H U 1979 Turbulent boundary layers, experiments, theory and modelling, AGARD-CP-271

Cebeci T, Stewartson K, Whitelaw J H 1984 *Numerical and physical aspects of aerodynamic flows II* (Berlin: Springer Verlag)

Chang P K 1976 *Control of flow separation* (New York: Hemisphere)

Chapman D R, Kuehn D M, Larson H K 1957 Investigation of separated flows in supersonic and subsonic streams with emphasis on the effect of transition, NACA TN 3869

Charwat A F 1970 *Advances in heat transfer* (eds) J P Hartnett, T F Irvine (New York: Academic Press) 6: 1–132

Chinneck A, Jones G C A, Tracey C M 1955 An interim report on the use of blowing to reduce fall in control effectiveness associated with shock-induced separation at transonic speeds, ARC 1756 FM 2231

Coe C F, Chyu W J, Dods J B 1973 Pressure fluctuations underlying attached and separated supersonic turbulent boundary layers and shock waves, AIAA Paper 73-996

Crawford D H 1961 The effect of air bleed on heat transfer and pressure distribution on 30° flares at a Mach number of 6·8, NASA TMX-439

Crocco L, Lees L 1952 *J. Aero. Sci.* 19: 649–676

Delery J M 1981 Investigation of strong shock-turbulent boundary layer interaction in 2-D transonic flows with emphasis on turbulence phenomena, AIAA Paper 81-1245

Delery J M 1983 *AIAA J.* 21: 180–185

Delery J M 1985 *Prog. Aerosp. Sci.* 22: 209–280
Dolling D S 1982 *AIAA J.* 20: 1385–1391
Dolling D S, Murphy M T 1983 *AIAA J.* 21: 1628–1634
Dolling D S, Or C T 1983 Unsteadiness of shock-wave structure in attached and separated compression corner ramp flow fields, AIAA Paper 83-1715
Don Gray J, Maus J R 1981 *AIAA J.* 19: 948–950
Driver D M, Lee Seegmiller H, Marvin J G 1983 Unsteady behaviour of a reattaching shear layer, AIAA Paper 83-1712
Eaton J K, Johnston J P 1982 *Turbulent shear flows.* 3. (eds) L J S Bradbury, F Durst, B E Launder, F W Schmidt, J H Whitelaw (Berlin: Springer Verlag)
Elfstrom G M 1972 *J. Fluid Mech.* 53: 113–127
Erdos J, Pallone A 1962 *Proc. Heat Transfer & Fluid Mech. Inst.* (Stanford: University Press)
Finke K 1975 Flow separation, AGARD-CP-168, Paper no. 28
Fukuda M K, Hingst W R, Reshotko E 1977 *AIAA J.* 14: 151–156
Gadd G E 1961 Interactions between normal shock waves and turbulent boundary layers, ARC R&M 3262
Gartshore J S, Newman B G 1969 *Aeronaut. Q.* 20: 25–56
Glusko G S 1965 *Bull. Acad. Sci. USSR Mech. Ser.* (no. 4): 13–23
Grande E, Oates G C 1973 Unsteady flow generated by shock-turbulent boundary layer interactions, AIAA Paper 73-168
Green J E 1970 *Prog. Aerosp. Sci.* 11: 235–340
Grin V T 1967 *Mech. Fluids Gases* 6: 115–117 (in Russian)
Henderson L F 1967 *J. Fluid Mech.* 30: 699–722
Horstmann C C, Hung C M 1979 Computation of three-dimensional turbulent separated flows at supersonic speeds, AIAA Paper 79-002
Horstmann C C, Owen F K 1974 *AIAA J.* 12: 1436–1438
Hubbart J E, Bangert L H Turbulent boundary layer control by a wall jet, AIAA Paper 70-107
Hung C M, Kordulla W 1983 A time split finite volume algorithm for three-dimensional flow field simulations, AIAA Paper 83-1957
Inger G R 1981 Transonic shock/turbulent boundary layer interaction and incipient separation on curved surfaces, AIAA Paper 81-1244
Inger G R, Mason W H 1976 *AIAA J.* 14: 1266–1272
Jones W P, Launder B E 1971 *Int. J. Heat Mass Transfer* 15: 301–314
Kistler A L 1964 *J. Acoust. Soc. Am.* 36: 543–550
Klineberg J M, Steger J L 1974 On laminar boundary layer separation, AIAA Paper 74-94
Kooi J W 1975 Flow separation, AGARD-CP-168, Paper no. 30
Kooi J W 1980 *Shock-boundary layer interaction in turbomachines*, Von Karman Inst. (Belgium), Lecture Series 1980-8
Krishnamurthy V 1973 *Suppression of shock-induced separation using tangential fluid injection: Part I*, M E Project Report, Dept. Aerosp. Eng., Indian Inst. Sci. Bangalore
Krogmann P, Stanewsky E, Thiede P 1984 Effect of local boundary layer suction on shock-boundary layer interaction and shock-induced separation, AIAA Paper 84-0098
Kuehn D M 1959 Experimental investigation of the pressure rise required for the incipient separation of turbulent boundary layers in two-dimensional supersonic flow, NASA Memo 1-21-59A
La Balleur J C 1981 Computation of viscous-inviscid interactions, AGARD CP 291, Paper No. 1
La Balleur J C 1984 *Numerical and physical aspects of aerodynamic flows II* (Berlin: Springer Verlag)
La Balleur J C, Blaise D 1985 *Rech. Aerosp.* (no. 4): 1–17
Lakshmikantha H, Yegna Narayan K, Srinivasan G 1969 Effect of fluid injection on shock-wave boundary layer interaction, Report 69 FM 7, Dept. Aerosp. Eng., Indian Inst. Sci., Bangalore
Law C H 1974 *AIAA J.* 12: 794–797
Lees L, Reeves B L 1964 *AIAA J.* 2: 1907–1920
Levy L L 1978 *AIAA J.* 14: 564–572
Lewis J E 1967 *Experimental investigation of supersonic laminar two-dimensional boundary layer separation in a compression corner with and without cooling*, Ph D thesis, Cal. Inst. Technol.
Lewis J E, Kubota T, Lees L 1968 *AIAA J.* 6: 7–14
Liepmann H W 1946 *J. Aeronaut. Sci.* 13: 623–637
Liepmann H W 1947 *J. Aeronaut. Sci.* 14: 295–302

Liepmann H W, Roshko A, Dhawan S 1951 On reflection of shock waves from boundary layers, NACA TN 2334

Lighthill M J 1953 *Proc R. Soc. London* A217: 478–507

Lock R C 1981 Computation of viscous-inviscid interactions, AGARD CP 291, Paper no. 2

Manjunath A R 1973 *Supression of shock-induced separation using tangential fluid injection: Part II*, M. E. Project Report, Dept. Aerosp. Eng., Indian Inst. Sci., Bangalore

Marvin J G 1982 Turbulence modelling for computational aerodynamics, AIAA Paper 82-0164

Marvin J G 1983 Modelling of turbulent separated flows for aerodynamic applications, NASA TM 84392

Mathews D C 1970 *Shock-wave boundary layer interactions in two-dimensional and axially-symmetric flows*, Ph D thesis, University of Washington

McCormack R W 1976 An efficient numerical method for solving the time-dependent compressible Navier-Stokes equations at high Reynolds number, NASA TM X-73129

McCormack R W 1982 *AIAA J.* 20: 1275–1281

McCormack R W, Lomax H 1979 *Annu. Rev. Fluid Mech.* 11: 289–316

McDevitt J B 1979 Supercritical flow about a thick circular-arc airfoil, NASA TM 78549

McDevitt J B, Levy L L, Deiwert G S 1976 *AIAA J.* 14: 606–613

McDonald H, Briley W R 1984 *Numerical and physical aspects of aerodynamic flows II* (Berlin: Springer Verlag)

Mehta U, Lomax H 1982 *Prog. Astronaut. Aeronaut.* 82: 297–375.

Meier G E A 1975 Flow separation, AGARD-CP-168, Paper no. 29

Melnik R E, Grossman B 1974 Analysis of interaction of a weak normal shock wave with a turbulent boundary layer, AIAA Paper 74-598

Melnik R E, Grossman B 1975 *Symp. Transonicum II* (Berlin: Springer Verlag)

Melnik R E, Grossman B 1977 *Transonic problems in turbomachinery* (New York: Hemisphere)

Messiter A F 1970 *SIAM J. Appl. Math.* 18: 241–257

Narasimha R 1978 Turbulent flow separation: Two problems in application oriented research, Report 78 FM 11, Dept. Aerosp. Eng., Indian Inst. Sci., Bangalore

Narasimha R, Prabhu A 1972 *J. Fluid Mech.* 54: 1–17

Narasimha R, Sreenivasan K R 1973 *J. Fluid Mech.* 61: 417–447

Neiland V 1969 *Fluid Dyn. (Engl. Transl.)* 4: 33–35

Oskam B, Vas I E, Bogdonoff S M 1975 Flow separation, AGARD-CP-168, Paper no. 41

Pate S R 1969 *AIAA J.* 7: 847–851

Peake D J 1966 The use of air injection to prevent separation of turbulent boundary layer in supersonic flow, ARC CP 890

Pearcey H H 1961 *Boundary layer and flow control* (ed.) G V Lachmann (New York: Pergamon) vol. 2

Plotkin K J 1975 *AIAA J.*13: 1036–1040

Purohit S C 1987a *J. Spacecraft Rockets* 23: 590–596

Purohit S C 1987b *AIAA J.* 25: 759–760

Rizetta D P, Burggraf O R, Jenson R 1978 *J. Fluid Mech.* 89: 535–552

Rose W C 1973 The behaviour of a compressible turbulent boundary layer in a shock-wave induced adverse pressure gradient, NASA TN D-7092

Rose W C, Johnson D A 1975 *AIAA J.* 13: 884–889

Roshko A, Thomke G J 1969 *Proc. Symp. on viscous interaction phenomena in supersonic and hypersonic flow* (Univ. of Dayton Press) pp. 109–138

Roshko A, Thomke G J 1976 *AIAA J.* 14: 873–879

Rotta J C 1968 Computation of turbulent boundary layers – 1968 AFOSR-IFP, Stanford Conference, vol I, pp 177–181

Rubesin M W 1982 The 1980–81 AFOSR-HTTM-Stanford Conference on Complex Turbulent Flows: Comparison of Computation and Experiment, vol II, pp 713–719

Sagdeo P M 1974 *Suppression of shock-induced separation using tangential fluid injection, Part III: Effect of injection slot*, M E Project Report, Dept. Aerosp. Eng., Indian Inst. Sci., Bangalore

Sandborn V A, Kline S J 1961 *J. Basic Eng. Trans. ASME* 83: 317–327

Sawyer W G, East L F, Nash C R 1977 A preliminary study of normal shock wave turbulent boundary layer interaction, RAE Tech. Memo Aero. 1714

Schlichting H 1968 *Boundary-layer theory* (New York: McGraw-Hill)

Schwendemann M F, Sanders B W 1982 Tangential blowing for control of strong normal shock-boundary layer interactions on inlet ramps, AIAA Paper 82-1082

Seddon J 1960 The flow produced by interaction of a turbulent boundary layer with a normal shock wave of strength sufficient to cause separation, ARC R&M 3502
Seddon J, Goldsmith E L 1985 *Intake aerodynamics* (New York: Collins)
Seebaugh W R, Childs M E 1970 *J. Aircraft* 7: 334–339
Seebaugh W R, Paynter G C, Childs M E 1968 *J. Aircraft* 5: 461–467
Settles G S, Bogdonoff S M 1982 *AIAA J.* 20: 782–789
Settles G S, Bogdonoff S M, Vas I E 1976a *AIAA J.* 14: 50–56
Settles G S, Perkins J J, Bogdonoff S M 1980 *AIAA J.* 18: 779–785
Settles G S, Vas I E, Bogdonoff S M 1976b *AIAA J.* 14: 1709–1715
Shang J S, Hankey W L 1975 *AIAA J.* 13: 1368–1374
Shang J S, Hankey W L, Law C H 1976 *AIAA J.* 10: 1451–1457
Simpson R L, Strickland J H, Barr P W 1977 *J. Fluid Mech.* 79: 553–594
Sirieix M 1975 Flow separation, AGARD-CP-168, Paper no. 12
Sirieix M, Delery J, Stanewsky E 1981 *Advances in fluid mechanics* (New York: Springer Verlag)
Stanewsky E 1973 *Transonic flows in turbomachinery*, Von Karman Institute (Belgium), Lecture Series 59
Stanewsky E, Nandanan M, Inger G R 1981 Computation of viscous-inviscid interactions, AGARD CP 291, Paper no. 4
Stewartson K 1974 *Adv. Appl. Mech.* 14: 145–239
Stewartson K, Williams P G 1969 *Proc. R. Soc. London* A312: 181–206
Sun C C, Childs M E 1974 *J. Aircraft* 11: 54–59
Tanner L H, Gai S L 1970 Effects of suction on the interaction between shock wave and boundary layer at a compression corner, ARC CP 1087
Tassa Y, Sankar N L 1979 *AIAA J.* 17: 1268–1270
Viegas J R, Horstmann C C 1978 Comparison of multi-equation turbulence models for several shock separated boundary layer interaction flows, AIAA Paper 78-1165
Veldman A E P 1984 *Computational methods in viscous flows* (ed.) W G Habashi (Gedney, NY: Pineridge) vol. 3
Viswanath P R, Brown J L 1983 *AIAA J.* 21: 801–807
Viswanath P R, Sankaran L, Sagdeo P M, Narasimha R 1977 Tangential blowing for control of shock-induced boundary layer separation: Review of recent IISc work, Report 77 FM 11, Dept. Aerosp. Eng., Indian Inst. Sci., Bangalore
Viswanath P R, Sankaran L, Sagdeo P M, Narasimha R, Prabhu A 1983 *J. Aircraft* 20: 726–732
Whitfield D L, Swafford T W, Jacocks J L 1981 *AIAA J.* 19: 1315–1322
Wilcox D C, Rubesin M W 1980 Progress in turbulence modelling for complex flow fields including compressibility effects, NASA TP-1517
Wong W F 1974 The application of boundary layer suction to suppress strong shock-induced separation in supersonic inlets, AIAA Paper 74-1063
Wong W F 1977 Application of boundary layer blowing to suppress strong shock-induced separation in supersonic inlets, AIAA Paper 77-147
Wong W F, Hall G R 1975 Suppression of strong shock boundary layer interaction in supersonic inlets by boundary layer blowing, AIAA Paper 75-1209
Yegna Narayan K, Narasimha R 1973 *Aeronaut. Q.* 24: 207–218